1D source term interactions for shallow lakes in SWAN

by

Sebastian Hartgring

Additional Graduation Work (CIE5050-09)

Student number:	4362063	
Project duration:	Oktober, 2021 – February, 2022	
First supervisor:	Dr. ir. M. Zijlema,	TU Delft
Second supervisor:	Prof. dr. A. J. H. M. Reniers,	TU Delft

TU Delft

Abstract

During the calibration of SWAN for shallow water lakes in the Netherlands, problems have been encountered. Especially the emergence of an unnatural, secondary peak in the low frequency part of the energy density spectrum poses problems. Therefore, this investigation aims to address the nonlinear shallow water source terms in SWAN that may introduce this artefact.

Firstly, the basics of linear wave theory and spectral modelling are introduced. Hereafter, these basics are extended to the modelling on nonlinear wave behaviour, as these phenomena form the basis of the relevant shallow water source terms.

The shallow water lake problem is reduced to a stationary, one dimensional problem, for which several model results are produced using varying parameters. Three main subjects can be identified: 1) the influence of depth-induced wave breaking using the BJ78-model or the $\beta - kd$-model, 2) the proportionality factor of the triad source term using the CCA-formulation, and 3) numerical properties such as frequency resolution and the magnitude of the flux limiter.

The results demonstrate that, for strong winds (U_{10} = 40 m/s) in shallow water (d = 2.5 m), source term interactions become complex as they are all of similar order of magnitude. Especially the interactions between triad wave-wave interactions and depth-induced wave breaking, and triads and quadruplets are important for determining the resulting wave spectrum. Increased wave breaking reduces the secondary peak but underestimates significant wave heights and dampens the spectrum. A more elaborate wave breaking formulation (the $\beta - kd$-model) showed improved performance, especially when it was set to allow younger wind waves (high kd) to develop.

Lowering the effect of the triad source term also removes the secondary peak, but may not be desirable as it is by definition a relevant shallow water source term. Reducing source term interactions by means of a stricter action limiter resulted in instabilities for the quadruplet source term and thus no convergence of the results.

A possible solution may be to investigate the possibility of reducing the effect of quadruplets for shallow water, as this term (together with the triad source term) contributes to the formation of the secondary peak. However, this has not been included in the scope of this investigation. Furthermore, improving the frequency resolution resulted in smoother spectra and less wiggles in the sum of the triad and quadruplet source terms. However, this may affect the performance of the quadruplet source term as this term has been calibrated for a fixed relative frequency resolution.

Contents

1 Introduction

The Netherlands contain a diverse landscape of waters consisting of lakes, rivers and tidal deltas (e.g. the Wadden Sea) with corresponding flood defences. Significant loads affecting these defences are wind waves generated by storms and the related wave-induced set-up of the water level, especially in lakes and lower river reaches. Therefore, numerical models are used to predict these waves for given wind climates. In the Netherlands, the Department of Waterways and Public Works (in Dutch: Rijkswaterstaat, abbreviated as RWS) makes use of the third-generation spectral wave model SWAN (Simulating WAves Nearshore).

Several SWAN models are used for these regions, each with specific settings for the source terms, boundary conditions and propagation terms. In order to strive for consistency between these models, Deltares is analysing their settings and output, and formulating an advice containing updated model settings. Important source term in the description of wind waves in shallow waters are the non-linear three-wave interactions (triads), which are caused by resonance between wave components in shallow water, and depth-induced wave breaking. In spite of an accurate mathematical description existing of the triad dynamics, difficulties are encountered when formulating an efficient and practical formulation for triads in wave models. As a result, inaccuracies can be encountered in model results and the formulated triad source term may not be always applicable. In this study, inaccuracies in the results of the spectral wave model SWAN are investigated and possible model improvements are assessed.

1.1. Problem description

In shallow water, nonlinear effects become relevant in shaping the energy density spectrum of the waves, such as triad wave-wave interactiond and depth-induced wave breaking. Currently, SWAN makes use of several models for triad modelling (LTA, SPB and CCA) and wave breaking (BJ78, BKD). During the validation of SWAN setting for the triad approximations in shallow lakes, some results contain the growth of a second peak in the lower frequencies of the energy-density spectrum (Groeneweg & Gautier, 2020; Groeneweg, 2021). The existence of this second peak is considered unnatural, thus leading to the conclusion that these model results are unreliable. Therefore, further analysis is required investigating the effect of the implementation of triad formulation with respect to the unnatural low frequency peak in order to identify and understand the limitations of the triad formulations in SWAN.

1.2. Research objective and questions

In order to decompose this problem, it is necessary to identify possible causes for the model result inaccuracies. Due to the limited time and resources available for an additional thesis, this study will focus on the implementation of the relevant source terms in SWAN (including the triads) and not verify the formulations of the triad and wave beraking formulations (see for example Bénit (2009) where a Distributed Collinear Triad Approximation was formulated as part of a Master's thesis). Instead, the calibration settings of the shallow water source terms are evaluated and the interactions between source terms are investigated. This leads to the following research questions for this investigation:

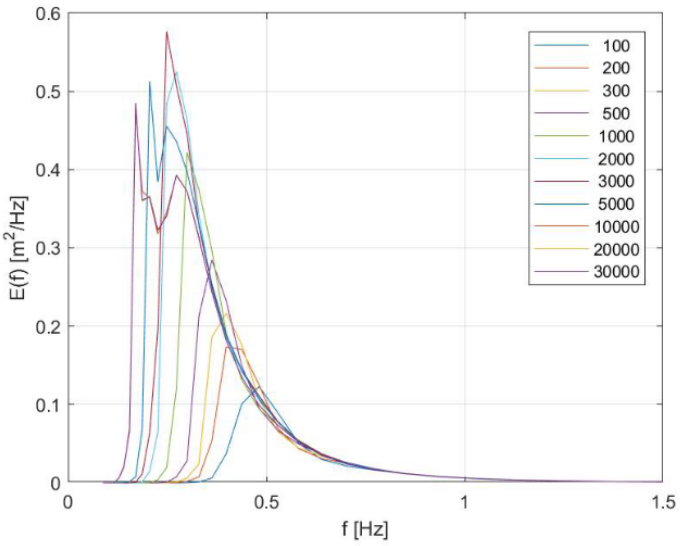

Figure 1.1: Appearance of second peak in energy density spectra for SWAN results after several distances using the CCA model in stationary 1D mode in SWAN for $U_{10} = 40m/s$, $d = 2.5m$, $L = 30km$ in SWAN. Obtained from Groeneweg (2021).

What are the limitations in the applicability of current shallow water source term formulations in SWAN for high wind speed conditions in shallow water?

- Which nonlinear effects affect waves propagating in shallow water?
- How are the triad wave-wave interactions and depth-induced wave breaking implemented in SWAN?
- Which other source terms are dominant in determining the energy density profile in shallow lakes?
- Which model conditions influence the applicability of the shallow water source term formulations?

The central question is supported by four secondary research questions. First, we consider the theoretical basis describing nonlinear effects of waves in shallow water. Secondly, we consider how triad formulations and depth-induced wave breaking are implemented in SWAN in order to understand the implementation and the effects of changing calibration settings. Thirdly, interactions with other source terms are considered as they may produce significant energy transfers and influence the shape of the spectrum. Finally, model conditions such as water depth and wind speed are assessed as they may pose limits in the applicability of certain source term formulations of SWAN.

1.3. Approach and structure

This investigation can be divided into five parts, as illustrated in figure 1.2. First, the current section contains the introduction to this investigation. In the second part, the theoretical background of the subject will be explored in chapter 2, followed by a description of the implementation of these concepts in SWAN in chapter 3. Chapters 4 and 5 form the two parts related to the use of SWAN model in this investigation. In chapter 4, the methodology of this investigation is treated. This section commences with a description of the selected case study, which is the Markermeer, and is followed by its implementation in the SWAN model and a description of the properties of the model that will be examined and varied between runs. Chapter 5 shows the results for the performed model runs, highlighting the two relevant source terms affecting the triads: the influence of wave breaking and the implementation of the quadruplet wave-wave interactions. Finally, the results of the SWAN model will be discussed in chapter 6 and followed by the conclusions and recommendations of this investigation.

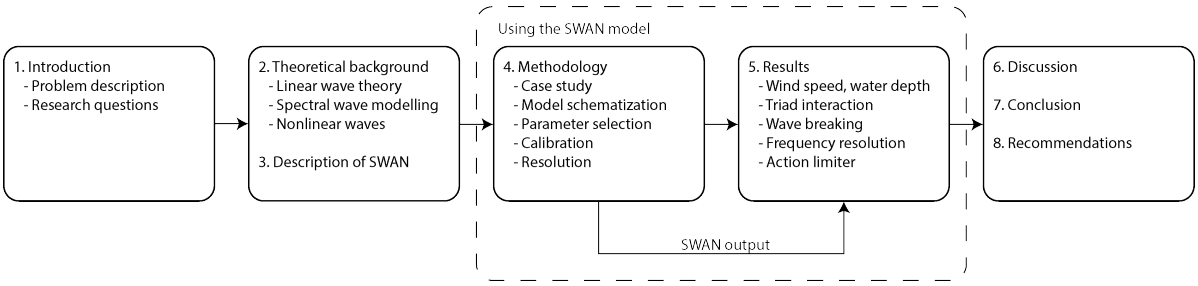

Figure 1.2: Structure of the chapters of this document.

2

Theoretical background

In this chapter the theoretical fundamentals of wave modelling will be described. A distinction can be made between phase-resolving models and phase-averaged models, both for linear and nonlinear wave theory. The first type describes the instantaneous state of motion of propagating waves ('solving each phase'), providing an extensive description of wave physics but also being computationally expensive. Phase-averaged models describe the average properties of the wave field, which is much more feasible allowing wave prediction over extensive areas (Eldeberky, 1996; Holthuijsen, 2007). The SWAN spectral wave model is of the latter class and used for wave prediction in the Netherlands, as it is able to describe wave properties for large lakes and coastal regions using relatively few computational resources (Holthuijsen et al., 1999).

Each type of model has its own advantages and results obtained using phase-averaged models can be used to improve formulations used in phase-resolving models and vice-versa. For example, a nonlinear phase-resolving model can be used to investigate triad wave-wave interactions with the objective of improving the formulation of nonlinear source terms in a phase-averaged model such as SWAN (Eldeberky, 1996). Additionally, deterministic descriptions of wave behaviour (e.g. wave breaking) can support and clarify its phase-averaged formulations. Therefore, both type of descriptions will be treated in this study.

Firstly, the fundamentals of linear wave theory are derived which describe the equations of motion for individual waves in linearised conditions, thus addressing the phase-resolving approach of wave modelling. Subsequently, linear wave theory is used to derive a phase-averaged formulation wave modelling, which also forms the theoretical basis of the SWAN spectral wave model. Hereafter, the linear descriptions of wave propagation will be extended with the objective of describing nonlinear wave interactions occurring in shallow water using the Boussinesq approximation and bispectral analysis for the phase-resolving and phase-averaged formulations respectively. Finally, the results of literature study concerning nonlinear phenomena of waves in shallow water are presented treating triad wave-wave interactions and wave breaking.

2.1. Linear wave theory

The derivation in this section is extensively based on the work by Holthuijsen (2007).

Free surface gravity waves propagating in oceanic waters can be described analytically by treating them as the large sum of independent harmonic waves, solving them for each phase. In order to obtain such an analytical solution for each harmonic wave, we have to derive the Laplace equation and linearised Bernoulli equation which describe the behaviour of the subjected water particles. Using these equations, characteristics of the propagation of surface waves can be described such as the velocity profile and the dispersion relationship. Linear wave theory also forms the basis for spectral wave modelling which will be treated in section 2.2.

2.1.1. Laplace and Bernoulli equation

Before formally deriving the relevant equations, it is necessary to set the frame of reference which they describe (figure 2.1). As this study primarily describes one-dimensional source terms of the spectral SWAN model, it is convenient to apply linear wave theory to a two-dimensional frame of reference with a horizontal

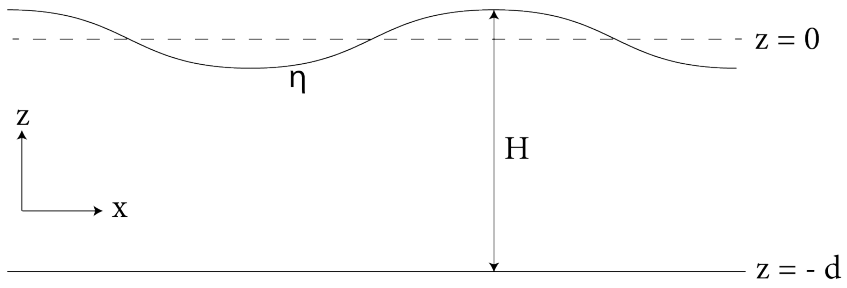

Figure 2.1: Frame of reference (own production).

x-axis and vertical z-axis. The water surface $\eta(x)$ is located at $z = \eta$, and a horizontal sea bed is considered at $z = -d$. This results in a water depth $H = d + \eta$ which, in linear wave theory, will be approximated to $H = d$ as $d >> \eta$. Furthermore, $z = 0$ is defined at the undisturbed water level.

Firstly, the conservation of volume of a control volume is described in terms of the horizontal flow velocity u_x and vertical flow velocity u_z. Assuming an incompressible fluid with constant density ρ, we obtain the continuity equation:

$$\frac{\partial u_x}{\partial x} + \frac{\partial u_z}{\partial z} = 0 \tag{2.1}$$

The conservation of momentum in horizontal direction is described by equation 2.2. This equation is obtained by balancing the total derivative of the momentum flux with the pressure gradient $\partial p/\partial x$. Similarly, the conservation of momentum in vertical direction is obtained (equation 2.3) with an additional term accounting for the gravitational force g.

$$\frac{\partial u_x}{\partial t} + \frac{\partial (u_x u_x)}{\partial x} + \frac{\partial (u_z u_x)}{\partial z} = -\frac{1}{\rho}\frac{\partial p}{\partial x} \tag{2.2}$$

$$\frac{\partial u_z}{\partial t} + \frac{\partial (u_x u_z)}{\partial x} + \frac{\partial (u_z u_z)}{\partial z} = -\frac{1}{\rho}\frac{\partial p}{\partial z} - g \tag{2.3}$$

Applying the chain rule to equations 2.2 and 2.3, and subtracting equation 2.1 results in the equations of motion described by equations 2.4 and 2.5.

$$\frac{\partial u_x}{\partial t} + u_x\frac{\partial u_x}{\partial x} + u_z\frac{\partial u_x}{\partial z} = -\frac{1}{\rho}\frac{\partial p}{\partial x} \tag{2.4}$$

$$\frac{\partial u_z}{\partial t} + u_x\frac{\partial u_z}{\partial x} + u_z\frac{\partial u_z}{\partial z} = -\frac{1}{\rho}\frac{\partial p}{\partial z} - g \tag{2.5}$$

In order to solve these equations, we need to define the related boundary conditions. At the upper boundary where $z = \eta$, we can consider a boundary condition which describes the motion of the water surface η. This kinematic surface boundary condition (equation 2.6) relates the vertical velocity u_z at the surface to the horizontal displacement of the surface $u_x \cdot \partial\eta/\partial x$ and the vertical velocity of the surface $\partial\eta/\partial t$. At the lower boundary where $z = -d$, we find the kinematic bottom boundary condition which describes that the water may not penetrate the impermeable bottom (equation 2.7). Furthermore, we define the dynamic boundary condition describing that the pressure at the surface equals zero which ensures that our surface waves are free waves and not forced (equation 2.8).

$$u_z = \frac{\partial \eta}{\partial t} + u_x\frac{\partial \eta}{\partial x} \quad \text{at} \quad z = \eta \tag{2.6}$$

$$u_z = 0 \quad \text{at} \quad z = -d \tag{2.7}$$

$$p = 0 \quad \text{at} \quad z = \eta \tag{2.8}$$

Additionally, we consider that the flow is irrotational (equation 2.9) and introduce the velocity potential function $\phi = \phi(x, z, t)$ as described in equation 2.10. Both considerations help us to rewrite the equation of motions into simpler forms.

$$\frac{\partial u_z}{\partial x} - \frac{\partial u_x}{\partial z} = 0 \tag{2.9}$$

$$u_x = \frac{\partial \phi}{\partial x} \quad \text{and} \quad u_z = \frac{\partial \phi}{\partial z} \tag{2.10}$$

First, we rewrite the continuity equation using the definition of the velocity potential resulting in the Laplace equation described by equation 2.11.

$$\frac{\partial^2 \phi}{\partial x^2} + \frac{\partial^2 \phi}{\partial z^2} = 0 \tag{2.11}$$

We can combine equations 2.4 and 2.5 with 2.9 and 2.10, change the order of differentiation and add the gz term to equation 2.4 (as $\partial(gz)/\partial x = 0$) and move all terms to the left-hand side, which results in the following equations:

$$\frac{\partial}{\partial x}\left[\frac{\partial \phi}{\partial t} + \frac{1}{2}\left(\frac{\partial \phi}{\partial x}\right)^2 + \frac{1}{2}\left(\frac{\partial \phi}{\partial z}\right)^2 + \frac{p}{\rho} + gz\right] = 0 \tag{2.12}$$

$$\frac{\partial}{\partial z}\left[\frac{\partial \phi}{\partial t} + \frac{1}{2}\left(\frac{\partial \phi}{\partial x}\right)^2 + \frac{1}{2}\left(\frac{\partial \phi}{\partial z}\right)^2 + \frac{p}{\rho} + gz\right] = 0 \tag{2.13}$$

As the term in the square brackets appears in both equations, we find that this term should equal zero, which results in the Bernoulli equation for unsteady motion. Neglecting the quadratic terms results in the linearised Bernoulli equation.

$$\frac{\partial \phi}{\partial t} + \frac{p}{\rho} + gz = 0 \tag{2.14}$$

This equation can be used to reformulate the dynamic surface boundary condition (equation 2.8) to the following form:

$$\frac{\partial \phi}{\partial t} + g\eta = 0 \quad \text{at} \quad z = 0 \tag{2.15}$$

In summary, the following equations and boundary conditions have been derived using a number of assumptions:

- Basic equations: Laplace and linearised Bernoulli
- Boundary conditions: two kinematic conditions at $z = \eta$ and $z = -d$, and one dynamic condition at $z = \eta$
- Key assumptions: the water is irrotational and incompressible with a constant density ρ

2.1.2. Flow velocities in deep and shallow water

A possible solution for the Laplace equation with the kinematic surface and bottom boundary conditions (is given by a harmonic wave with amplitude a propagating in x-direction (equation 2.16) and the corresponding velocity potential function (equation 2.17):

$$\eta(x,t) = a\sin(\omega t - kx) \tag{2.16}$$

$$\phi = \frac{\omega a}{k}\frac{\cosh[k(d+z)]}{\sinh(kd)}\cos(\omega t - kx) \tag{2.17}$$

The velocity potential function can be rewritten to obtain the velocity functions of the water particles:

$$u_x = \hat{u}_x \sin(\omega t - kx) \quad \text{where} \quad \hat{u}_x = \omega a \frac{\cosh[k(d+z)]}{\sinh(kd)} \tag{2.18}$$

$$u_z = \hat{u}_z \sin(\omega t - kx) \quad \text{where} \quad \hat{u}_z = \omega a \frac{\sinh[k(d+z)]}{\sinh(kd)} \tag{2.19}$$

The solution in equation 2.17 demonstrates the influence of the water relative water depth on the behaviour of the free surface wave, through the effect of kd in the velocity potential function. It is possible to distinguish two extreme regimes in which the wave propagates: deep water where $kd \to \infty$ and shallow water where $kd \to 0$. In deep water, the functions of the velocity magnitude reduce to:

$$\hat{u}_x = \omega a \exp(kz) \quad \text{and} \quad \hat{u}_z = \omega a \exp(kz) \tag{2.20}$$

The total velocity of the particle remains constant (as $\hat{u}_x = \hat{u}_z$ and $\sin(\omega t - kx)^2 + \cos(\omega t - kx)^2 = 1$) and reduces exponentially for water particles situated further from the water surface. The displacement of the water particles is described by a circular path, called the orbital motion, and the water depth itself no longer

influences the velocity profile of the surface waves. Or, worded differently, the waves 'do not feel the bottom'.

An alternative situation emerges when observing the waves in shallow water. For $kd \to 0$, the velocity magnitudes simplify to the following form:

$$\hat{u}_x = \frac{\omega a}{kd} \quad \text{and} \quad \hat{u}_z = \omega a\left(1 + \frac{z}{d}\right) \tag{2.21}$$

This result shows that the horizontal velocity magnitude is constant over the water depth and that it increases for smaller water depths. The waves 'feel the bottom' and the orbital motion observed in deep water has changed to the trajectory of an ellipse which flattens towards the bottom. Eventually, vertical accelerations can be neglected and the wave can be described by the shallow-water equations.

2.1.3. Dispersion relationship

In addition to the Laplace equation and the kinematic boundary conditions, the linearised Bernoulli equation and the dynamic surface boundary condition can provide insights in the dynamic behaviour of surface gravity waves. For this, the solution of the solution for the velocity potential function (equation 2.17) is combined with the reformulated dynamic boundary condition (equation 2.15), where it is assumed that $\sinh(k\eta + kd) \approx \sinh(kd)$. This results in the dispersion relationship:

$$\omega^2 = gk\tanh(kd) \tag{2.22}$$

The dispersion relationship describes the relationship between the wave number and the radian frequency for each wave. It can be used to find the phase velocity of the waves using $c = \omega/k$:

$$c = \sqrt{\frac{g}{k}\tanh(kd)} \tag{2.23}$$

This shows that longer waves travel faster than shorter waves, which results in the so-called dispersive behaviour of the wave field. Again considering the limit state of shallow water for which $kd \to 0$, we obtain the following expression for the dispersion relationship and the phase speed:

$$\omega = k\sqrt{gd} \quad \text{and} \quad c = \sqrt{gd} \tag{2.24}$$

The phase speed becomes independent of the wave number resulting in non-dispersive waves and the dispersion relationship becomes a linear function for a constant water depth. We will observe in section 2.3.3 that this property for free waves in shallow water has important implications for processes relevant in distributing wave energy in shallow water.

Individual waves propagate with the phase velocity $c = \omega/k$, but we should also consider the group velocity $c_g = \partial\omega/\partial k$ which describes the speed at which wave groups, and thus wave energy, propagates. Using the dispersion relationship one obtains:

$$c_g = \frac{\partial\omega}{\partial k} = nc \quad \text{where} \quad n = \frac{1}{2}\left(1 + \frac{2kd}{\sinh(2kd)}\right) \tag{2.25}$$

2.2. Spectral wave modelling

The derivation in this section is extensively based on the work by Holthuijsen (2007).

Spectral wave models, such as SWAN, provide an averaged solution for simulated wave records and do not solve for the individual waves. In order to understand the background of such models, this section describes the basic theory behind spectral wave modelling.

2.2.1. Variance density spectrum

As mentioned before, it may be more feasible for models to describe averaged wave statistics instead of individual waves. The basic assumption for this approach is that the surface elevation of the ocean is a stationary, Gaussian process, which is a reasonable assumption for wave records of limited duration (15-30 minutes) (Holthuijsen, 2007). In this approach, the surface elevation of the ocean is considered to be the

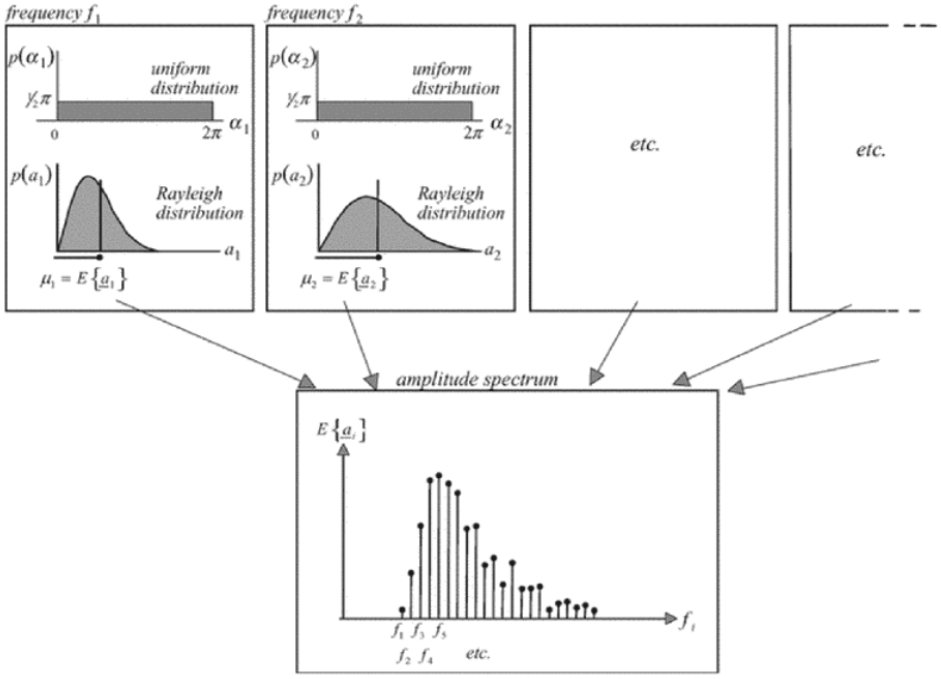

Figure 2.2: The random-phase/amplitude model, demonstrating how realisations of the phase and amplitude per frequency result in a discrete amplitude spectrum. Obtained from Holthuijsen (2007).

sum of a large number of harmonic waves, each with a random amplitude and phase , which results in the formulation of the random-phase/amplitude model (in one dimension):

$$\eta(t) = \sum_{i=1}^{N} a_i \cos(\omega_i t + \alpha_i) \tag{2.26}$$

The phases and amplitudes are described b their probability density functions, where the phase α_i is uniformly distributed between 0 and 2π, and the amplitude a_i follows a Rayleigh distribution. Due to the properties of these processes, it is possible to describe a wave records by drawing values for the phase and amplitude for each frequency, and display the expected value for the amplitude using the amplitude spectrum $E\{a_i\}$ (see figure 2.2). The energy of a wave field is proportional to its variance ($E_{total} = \rho g \eta^2$), which makes it more convenient to describe the wave field by $E\{\frac{1}{2}a_i^2\}$. Furthermore, the amplitude spectrum is based on discrete frequencies, while in practice the frequency range is a continuous function, which can be solved by distributing the variance $E\{\frac{1}{2}a_i^2\}$ over the frequency interval Δf_i. Taking the limit for Δf_i results in the description of the variance density spectrum:

$$E(f) = \lim_{\Delta f \to 0} \frac{1}{\Delta f} E\left\{\frac{1}{2}a^2\right\} \tag{2.27}$$

The variance density spectrum describes how wave energy is distributed over the frequencies in the wave field. One can obtain the energy density spectrum from $E(f)$ by multiplying its values with ρg. As a result, the shape of the spectrum provides information about the type of waves present in the wave field. For example, a narrow spectrum indicates that the present waves are regular, while a broad spectrum describes an irregular wave field, and a spectrum with two frequency peaks, one low and one high, may indicate the presence of both wind and swell waves. When the two-dimensional spectrum is considered, the direction of the wave field θ is also included for which $E(f) = \int_{-\pi}^{\pi} E(f,\theta) d\theta$.

2.2.2. Characteristic values of a wave spectrum

From the variance density spectrum, characteristic values of the wave field can be obtained using the moments of the wave spectrum and the probability density function of the wave height. The n-th moment of the wave spectrum is defined as:

$$m_n = \int_0^{\infty} f^n E(f) df \quad \text{for} \quad n = ..., -3, -2, -1, 0, 1, 2, 3, ... \tag{2.28}$$

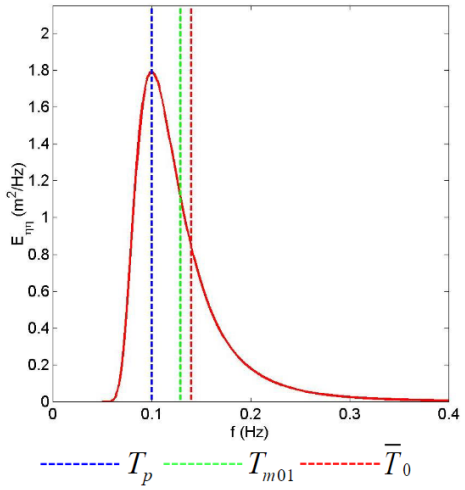

(a) Characteristic wave periods of a wave record, drawn in the variance density spectrum.

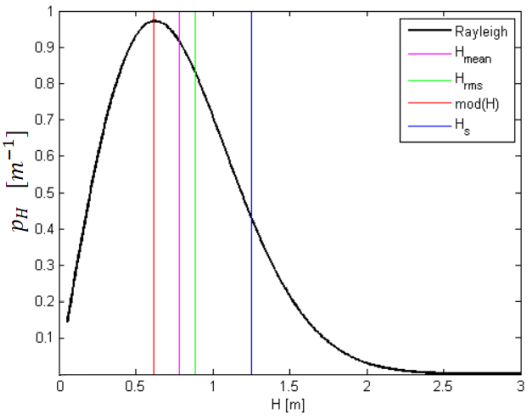

(b) Characteristic wave heights of a wave record, drawn in the Rayleigh distribution.

Figure 2.3: Characteristic statistical values for a wave record. Obtained from Tissier & Reniers (2021)

Furthermore, the probability function of the wave height H is Rayleigh-distributed and has the following form:

$$p(H) = \frac{H}{4m_0} \exp\left(-\frac{H^2}{8m_0}\right) \tag{2.29}$$

Holthuijsen (2007) shows that, using these two equations, the following statistical characteristics of the wave spectrum can be obtained (as illustrated in figure 2.3):

- The mean zero-crossing period: $\overline{T_0} = T_{m02} = \sqrt{\frac{m_0}{m_2}}$
- The mean wave period: $T_{m01} = \left(\frac{m_0}{m_1}\right)$
- The peak period: $T_p = \frac{1}{f_p}$ for which $E(f = f_p) = \max(E(f))$
- The spectral wave period: $T_{m-10} = \left(\frac{m_{-1}}{m_0}\right)$
- The mean wave height: $\overline{H} = \sqrt{2\pi m_0}$
- The root-mean-square wave height: $H_{rms} = \sqrt{8m_0}$
- The significant wave height: $H_s = H_{m0} \approx 4\sqrt{m_0}$
- The most probable wave height: $\text{mod}\,(H) = 2\sqrt{m_0}$

These wave height formulations obtained from the spectrum each have their own applicability and practical use, but are also used for discrete wave observations. For example, the root-mean-square wave height for observed waves is defined as $H_{rms} = \left(\frac{1}{N}\sum_{i=1}^{N} H_i^2\right)^{1/2}$ and is related to the total energy of the spectrum, and the significant wave height, defined as the mean of the highest one-third of waves, has shown to be close to the values of visually estimated wave heights (Holthuijsen, 2007). Similarly for wave periods, recently one prefers using T_{m-10} over the 'old-fashioned' T_p as it is the equivalent period needed to calculate the energy flux of the wave field and more closely related to wave overtopping (Olieman, 2011; Hofland et al., 2017).

It should be taken into account that spectral models may be shown to under- and overestimate modelled wave heights and periods when compared to direct measurements, including the SWAN model treated in this investigation. Furthermore, the mathematical descriptions based on the wave spectrum are assumed for a wave field described by Gaussian processes and being Rayleigh distributed, which poses problems for waves in near-shore conditions where both descriptions may be violated (Battjes & Groenendijk, 2000).

2.3. Nonlinear waves in shallow water

Linear wave theory describes the wave field as the sum of several harmonic waves propagating freely which, in deep water, has proven to be a reliable description. However, the validity of linear wave theory becomes questionable when the waves enter shallow water. This is illustrated by observing the simplification used in deriving the dispersion relationship (section 2.1.3) where it was assumed that $\sinh(k\eta + kd) \approx \sinh(kd)$. As explained by Dingemans (1994), this will result in two restrictions for the linearisations used in deriving the linear wave theory equations: for shallow water waves, the wave amplitude must be small compared to the water depth ($|\eta| << d$) and for deep water waves, the wave steepness must be small ($k|\eta| << 1$). The nonlinearity of a wave can be quantified using the Ursell number which is the ratio between wave steepness and the relative depth:

$$N_{Ursell} = \text{steepness}/(\text{relative depth})^3 = (H/L)/(d/L)^3 = HL^2/d^3 \tag{2.30}$$

An alternative formulation can be obtained using wave-averaged variables, as used for biphase calculations in SWAN (Holthuijsen, 2007). Using $L = cT$ and the shallow water wave speed $c = \sqrt{gd}$, one obtains :

$$N_{Ursell} = \frac{gH_{m0}\overline{T}^2}{8\sqrt{2}\pi^2 d^2} \tag{2.31}$$

In the case of wind waves generated in shallow water, these waves may initially satisfy both criteria as the young waves have a low height which implies a large relative water depth. However, as the waves grow due to the presence of wind, they may reach a wave height for which $\mathcal{O}(|\eta|) = \mathcal{O}(d)$, resulting in an inaccurate description of free wave propagation when using linear wave theory.

Therefore, it is necessary to include nonlinear effects in both phase-resolving and phase-averaged models. For phase-resolving, an approximation based on the theory of Boussinesq can be used to describe the nonlinear behaviour of the waves. Alternatively,bispectral analysis can be used to describe the bispectrum which quantifies the nonlinearity of the wave field in an phase-averaged approach, forming the basis for describing nonlinear triad wave-wave interactions in the phase-averaged model SWAN (Eldeberky & Battjes, 1995; Becq-Girard et al., 1999; Salmon et al., 2016).

2.3.1. The Boussinesq approximation

The Laplace equation can be solved alternatively, which will produce a solution including nonlinear terms thus providing a basis for nonlinear phase-resolving models. Following the original derivation from Boussinesq (1872), as described by Dingemans (1994), we integrate the Laplace equation (equation 2.11) twice with respect to z which results in the use of the depth-averaged horizontal flow velocity u_0. Furthermore, we approximate the horizontal velocity to be constant over the vertical, which allows us to obtain the following two equations:

$$\frac{\partial \eta}{\partial t} + \frac{\partial}{\partial x}\left[(d+\eta)u_0\right] = \frac{1}{6}d^2\frac{\partial^3 u_0}{\partial t \partial x^2} \tag{2.32}$$

$$\frac{\partial u_0}{\partial t} + u_0\frac{\partial u_0}{\partial x} + g\frac{\partial \eta}{\partial x} = \frac{1}{2}d\frac{\partial^3 (d u_0)}{\partial t \partial x^2} \tag{2.33}$$

These equations describe the water waves in the transition zone from deep water to shallow water. It is interesting to note that setting the high-order terms to zero in equations 2.32 and 2.33 will result in the shallow water equations.

In addition to the original derivation by Boussinesq (1872), several alternative forms of Boussinesq-type equations have been formulated which can be used to describe nonlinear effects in waves or improve the range of validity for the equations (Herbers & Burton, 1997). Similarly to linear wave theory, it is possible to derive a dispersion relationship based on each of the Boussinesq-type equations. Madsen et al. (1991) have compared several forms of these dispersion relations and formulated a general expression described by equation 2.34, where B corresponds to a value specific value related to the formulation. For example, $B = 0$ corresponds to the solution for the classical Boussinesq-equations. Note that in shallow water, equation 2.34 reduces to the dispersion relationship for shallow water (equation 2.24).

$$\frac{c^2}{gh} = \frac{1 + Bk^2h^2}{1 + (B + 1/3)\,k^2h^2} \tag{2.34}$$

Madsen et al. (1991) compared these several forms with an analytical solution obtained using a polynomial expansion of Stokes first-order theory and concluded that the formulation using $B = 1/15$ provided the best linear dispersion characteristics. Their formulation of the Boussinesq-type equations differs from the classical formulation of Boussinesq (1872) which emerges when using $B = 0$. An accurate description of the dispersion characteristics is important as they describe the mechanics that govern nonlinear wave interactions and provide a better prediction for the phase speed of waves which have become asymmetric and skewed due to these nonlinear interactions (Eldeberky, 1996). Furthermore, phase-resolving models based on Boussinesq-type equations have shown to be very useful for investigating nonlinear effects in shallow waters such as wave breaking and triad wave-wave interactions (see Eldeberky (1996) for several examples).

2.3.2. Bispectral analysis

Bispectral analysis can be used to examine nonlinear processes in shallow water waves such as energy transfers and wave breaking (K. Hasselmann et al., 1963; Eldeberky, 1996). Spectral analysis of zeroth-order moments, as described in section 2.2, is based on the analysis of the amplitudes in the wave field and is independent of the phases. This is important, as otherwise the sea surface elevation could not be considered a Gaussian process which is fundamental for linear wave theory (K. Hasselmann et al., 1963). However, this poses problems for investigating nonlinear interactions between waves in the wave field as it is unclear whether the observed waves are independently generated or nonlinearly coupled (Kim et al., 1980). Therefore, higher-order spectra such as the bispectrum provide a solution as they analyse phase-coherence between waves in the spectrum which provides an indication of the presence of nonlinear coupling between the waves, as introduced by K. Hasselmann et al. (1963).

In order to obtain a definition for the bispectrum, we rewrite the sea surface elevation as the sum of spatially varying Fourier components (similar to a summation of the definition used for an individual wave in equation 2.16) following Eldeberky (1996):

$$\zeta(x,t) = \sum_{p=-\infty}^{\infty} C_p(x) \exp\left[-i\left(\omega_p t\right)\right] \tag{2.35}$$

In this formulation, p is the rank of the harmonic and C_p is the complex Fourier amplitude. Using equation 2.35, the bispectrum B can be defined as:

$$B(\omega_1,\omega_2) = \left[\frac{1}{2\pi}\right]^2 \int_{-\infty}^{+\infty} R(\tau_1,\tau_2) \exp\left[-i\left(\omega_1\tau_1 + \omega_2\tau_2\right)\right] d\tau_1 d\tau_2 \tag{2.36}$$

in which

$$R(\tau_1,\tau_2) = \langle \zeta(t)\zeta(t+\tau_1)\zeta(t+\tau_2)\rangle \tag{2.37}$$

Considering three waves with radian wave frequencies ω_1, ω_2 and ω_{1+2}, the value for the bispectrum will indicate the nonlinear coupling between the waves. When the phases between the waves are randomly distributed (over $-\pi$ and π), the bispectrum will vanish, while nonlinear coupling will result in correlated phases and thus a non-zero value for the bispectrum.

In practice, it is more convenient to express the bispectrum in terms of a normalized amplitude b and a phase β (Kim & Powers, 1979; Doering & Bowen, 1986; Eldeberky, 1996). The normalized amplitude is bounded by zero and one ($0 \leq b \leq 1$), where the lower boundary indicates no correlation between the waves while the upper boundary indicates full coupling as illustrated by figure 2.4 (Kim & Powers, 1979).

$$b_{1,2}^2 = \frac{\left|B_{1,2}\right|^2}{\left\langle |C_1 C_2|^2 \right\rangle \left\langle |C_{1+2}|^2 \right\rangle} \tag{2.38}$$

The biphase is defined as the angle between the real and imaginary part of the bispectrum (equation 2.39) and tends to be uniformly distributed for uncorrelated waves ($-\pi \leq \beta \leq \pi$). In shallow water, triad resonance occurs and the biphase becomes concentrated between 0 and $-\frac{1}{2}\pi$, simultaneously indicating nonlinear behaviour as a biphase of $-\frac{1}{2}\pi$ is associated with a wave shape pitched forward (Eldeberky & Battjes, 1995).

$$\beta(\omega_1,\omega_2) = \tan^{-1}\left\{\frac{\Im\left[B(\omega_1,\omega_2)\right]}{\Re\left[B(\omega_1,\omega_2)\right]}\right\} \tag{2.39}$$

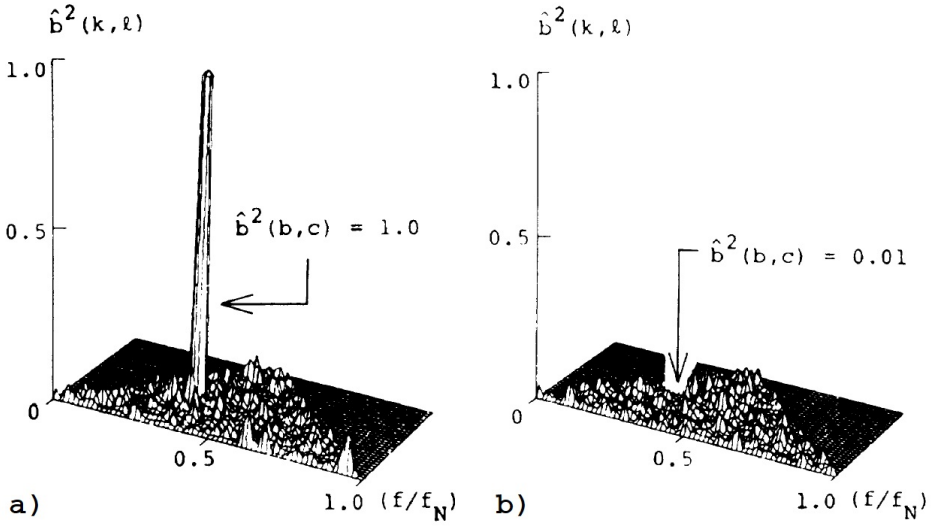

Figure 2.4: The squared normalized amplitude b^2 versus the frequency normalized by the Nyquist frequency f/f_N for a) a signal consisting three waves with consistent phases ($\phi_{b+c} = \phi_b + \phi_c$) and b) independent waves, both including Gaussian background noise. Obtained from Kim & Powers (1979).

Not surprisingly, the biphase is shown to be correlated to the Ursell number (figure 2.5), an indication for nonlinearities of waves (Doering & Bowen, 1995; Eldeberky & Battjes, 1995). As a result, the mean value of the biphase $\overline{\beta}$ has been defined as (Holthuijsen, 2007):

$$\overline{\beta} = -\pi + \pi \tanh(\delta / N_{Ursell}) \tag{2.40}$$

2.3.3. Nonlinear wave-wave interactions

Sections 2.3.1 and 2.3.2 described how wave propagation formulations can be extended to included nonlinear effects, using either a phase-resolving or phase-averaged approach. An important source of nonlinear energy transfer in the wave field is the nonlinear wave-wave interactions. These harmonics are generated when resonance conditions are met for the frequencies and wave numbers of travelling waves. Two examples of such transfers are the triad wave-wave interactions describing resonance between three waves (figure 2.6), and quadruplet wave-wave interactions describing resonance between four waves (figure 2.7).

Quadruplet wave-wave interactions occur when matching of frequencies and wave number occur between two pairs of free waves. This can be described mathematically as follows (for one dimension):

$$\omega_1 + \omega_2 = \omega_3 + \omega_4 \quad \text{and} \quad k_1 + k_2 = k_3 + k_4 \tag{2.41}$$

Similarly, it is possible to describe resonance conditions for triad wave-wave interactions:

$$\omega_1 + \omega_2 = \omega_3 \quad \text{and} \quad k_1 + k_2 = k_3 \tag{2.42}$$

These requirements illustrate the importance of the dispersion relationship as it describes the possible combinations of wave number and radian frequency for free waves. In deep water, the resonance condition for triads cannot be satisfied as the dispersion curve has negative curvature. This means that for a surface gravity wave with the property $\omega_3 = \omega_1 + \omega_2$, the corresponding wave number, described by the dispersion relationship, will always $k_3 \neq k_1 + k_2$ and vice-versa (figure 2.9a). Therefore, nonlinear wave-wave interactions in deep water are only described by quadruplet wave pairs (or higher order resonance pairs) (K. Hasselmann et al., 1994). However, in shallow water propagating waves become less dispersive therefore resulting in a smaller mismatch for the resonance conditions (figure 2.9b) (Madsen & Sorensen, 1993). Even for near-resonance conditions, energy transfer and phase-coupling can occur and result in observable energy transfers (Holthuijsen, 2007), and shoaling effects may enhance these processes as they reduce the mismatch even further (Herbers & Burton, 1997).

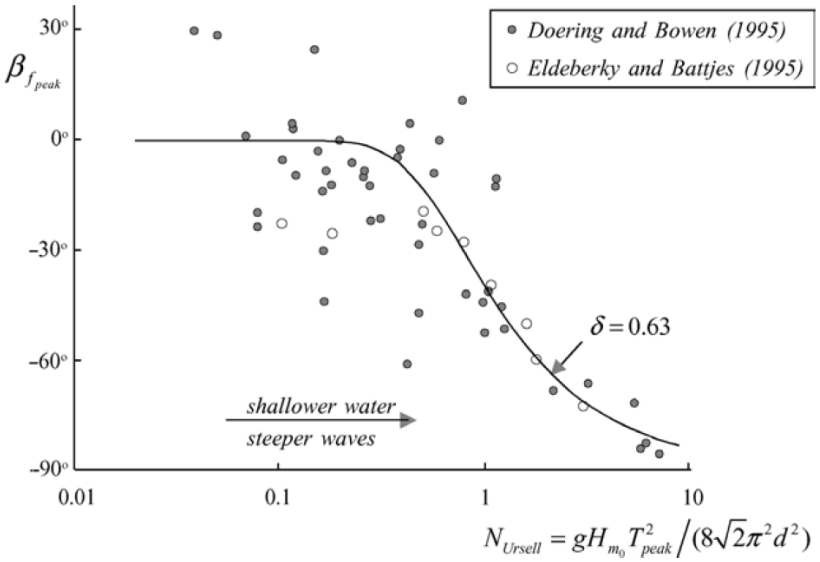

Figure 2.5: The observed biphase in experiments by Doering & Bowen (1995) and Eldeberky & Battjes (1995) at the peak for waves propagating into shallow water. Obtained from Holthuijsen (2007).

The triad and quadruplet wave-wave interactions show distinct behaviour with regards to their transfer of energy within the spectrum. The energy gain or loss of a component of the quadruplet waves can be described by the Boltzmann equation for four-wave resonant interactions, as described in the textbooks by K. Hasselmann et al. (1994) and Holthuijsen (2007), and solving for these equations for a typical JONSWAP spectrum results in a distinct shape of the redistribution due to the quadruplets with a low value at the peak frequency (figure 2.8a). On the other hand, triads have been shown to be stronger for interactions between the wind peak frequency f and its higher harmonics (e.g. (f,f), $(f,2f)$, $(2f,2f)$, etc.) (Doering & Bowen, 1986). As a result, the energy transfers of triad wave-wave interactions concentrate primarily around the peak frequency, transferring energy from f to $2f$, as illustrated by figure 2.8b. The concentration around the harmonics of the peak frequency allows for simplifications in the formulation of triad source terms in spectral models, as the situation can be approximated by only considering wave-wave interactions between the peak frequencies (Eldeberky & Battjes, 1995). By definition, as energy is only transferred due to nonlinear wave-wave interactions, the triad and quadruplet source terms only redistribute energy over the spectrum and action, momentum and energy remain conserved (K. Hasselmann et al., 1994).

These resonance conditions further underline the importance of an accurate approximation of the dispersion relation, as several forms can be obtained with varying errors as described by Madsen & Sorensen (1993). Still, one should also note that even the dispersion relationship of equation 2.34 using $B = 1/15$ may underestimate nonlinearities for high values of kh as it is based on the Boussinesq-approximation and thus optimized for waves in intermediate and shallow water depths (Herbers & Burton, 1997; Becq-Girard et al., 1999). Therefore, Herbers & Burton (1997) highlights the possibility of supplementing Boussinesq-theory by, for example, finite depth theory in order to span several depth regions. Alternatively, Abreu et al. (1992) describe triad interactions through a statistical model with a limited validity for shallow water. While the model was able to capture nonlinear physics, difficulties emerged when incorporating the description of quadruplet wave-wave interactions as a result of disjoint time scales.

Furthermore, it is essential to distinguish between waves that are generated as a result of nonlinear energy transfers or independent waves that are spontaneously excited but also fit the resonance criteria. Consequently, the bispectrum can be used to identify waves generated by nonlinear energy transfers as the phase coherence between the waves is an indication of triad wave-wave interactions (Kim et al., 1980).

As the quadruplet wave-wave interactions are distinctly a deep water term while the triads only appear in shallow water (Madsen & Sorensen, 1993), the question can be raised whether quadruplet terms should be

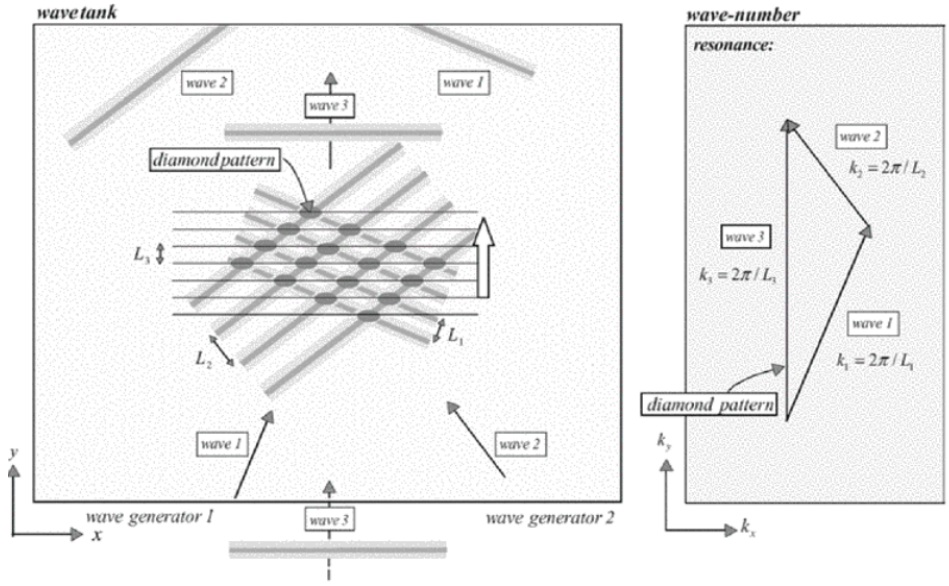

Figure 2.6: Wave-wave interactions as a result of resonance between triad wave components. Obtained from Holthuijsen (2007).

included for shallow water simulations. Van der Westhuysen (2007) hypothesised that the current formulations of quadruplet terms in models are derived for deep water which are therefore violated in shallow water. At the same time, the triad source term remains weak in deep water and increases as the depth decreases. A possible solution is to deactivate quadruplet interactions in strongly nonlinear wave field based on the Ursell number Van der Westhuysen (2007) (for example, $Ur > 0.1$), which is a suitable quantity for parameterizing wave-wave interaction Doering & Bowen (1986).

However, Bottema (2001) argues that partial deactivation of quadruplet interaction can lead to poor iteration behaviour in some situations, making it preferable that the triad and quadruplet terms should remain active alongside each other. Additionally, he dispersion relation for the free and bound waves plays an important role for these near-resonant interactions. It may be possible that the primary wave finds itself in shallow water and experiences triad wave-wave interactions, while higher harmonics of this wave find themselves in relatively deeper water and thus should be subjected to quadruplet wave-wave interactions. Madsen & Sorensen (1993)

2.3.4. Wave breaking

Another important nonlinear source of wave energy redistribution is wave breaking. The height of propagating waves can increase, for example as a result of wind input in deep water or shoaling in shallow water. However, one may expect that the height of a wave is limited to a maximum as a result of stability criteria affecting the wave. For example, Miche (1944) has shown, using Stokes wave theory, that a theoretical height limit can be derived based on the fact that the particle velocity u_x of the wave may not exceed its celerity c, as this would result in an unstable wave:

$$H_{max} \approx 0.14 L \tanh\left(\frac{2\pi d}{L}\right) \tag{2.43}$$

This approximates in deep and shallow water to $H_{max} \approx 0.14L$ and $H_{max} \approx 0.88d$ respectively and corresponds to a maximum crest angle of 120 degrees (figure 2.11), as shown initially by Stokes (1880) (Longuet-Higgins, 1963; Bosboom & Stive, 2022). Similarly, Longuet-Higgins (1969) describes a theoretical limit for waves in deep water based on the vertical acceleration at the crest exceeding $g/2$:

$$H_{max} = \frac{a}{2}\left\{\frac{1}{2} g/(a\omega^2)\right\} \tag{2.44}$$

Wave breaking near shorelines can be characterised using the Iribarren parameter ξ which represents the ratio of the beach slope $\tan(\alpha)$ and the deep water wave steepness H_0/L_0 (Bosboom & Stive, 2022). This

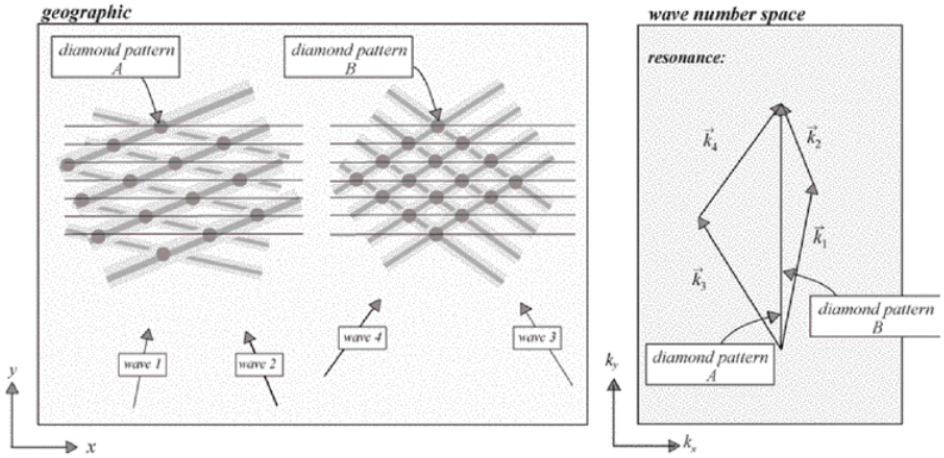

Figure 2.7: Wave-wave interactions as a result of resonance between quadruplet wave components. Obtained from Holthuijsen (2007).

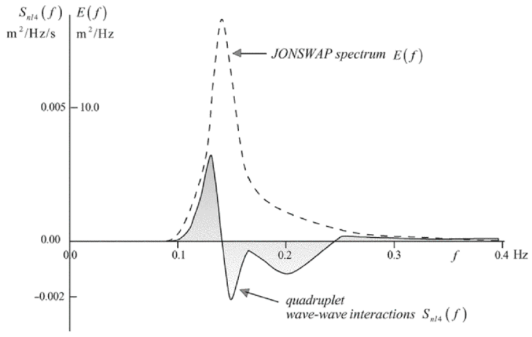

(a) The characteristic shape of energy redistribution by quadruplet wave-wave interactions in deep water for a JONSWAP-shaped spectrum.

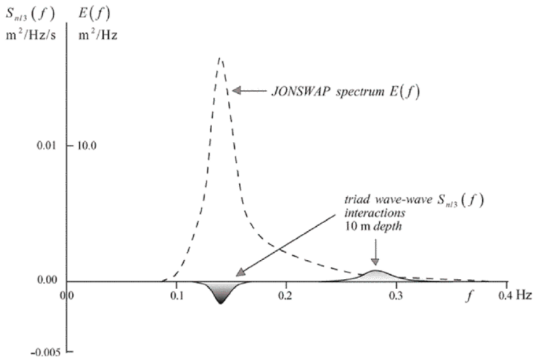

(b) The characteristic shape of energy redistribution by triad wave-wave interactions in shallow water for a JONSWAP-shaped spectrum.

Figure 2.8: Comparison between the quadruplet and triad source term. Obtained from Holthuijsen (2007).

ratio was first used by Canavilles & Nogales (1949) and elaborated on by Battjes (1974), who described its importance for defining the type of wave breaking occurring at the beach (i.e. surging, collapsing, plunging and spilling breakers).

$$\xi = \frac{\tan(\alpha)}{\sqrt{H_0/L_0}} \tag{2.45}$$

Observations show that the limit proposed by Miche (1944) functions as an upper limit, but wave breaking dynamics remain difficult to describe for both phase-resolving and phase-averaged models due to its nonlinear behaviour and the scarcity of solutions for realistic wave fields (T. T. Janssen, 2006; Van der Westhuysen, 2007; Salmon, 2016). In practice, spectral models often make a distinction between instability-induced breaking occurring in deep water (white-capping) and depth-induced wave breaking in shallow water, where each source term describes the dissipation based on an empirical or parametric relation (Holthuijsen, 2007). This is especially valid for depth-induced wave breaking, for which many formulations exist which are proven to be inconsistent with theory, observations and model predictions, for example in the case of horizontal bathymetries (Salmon, 2016).

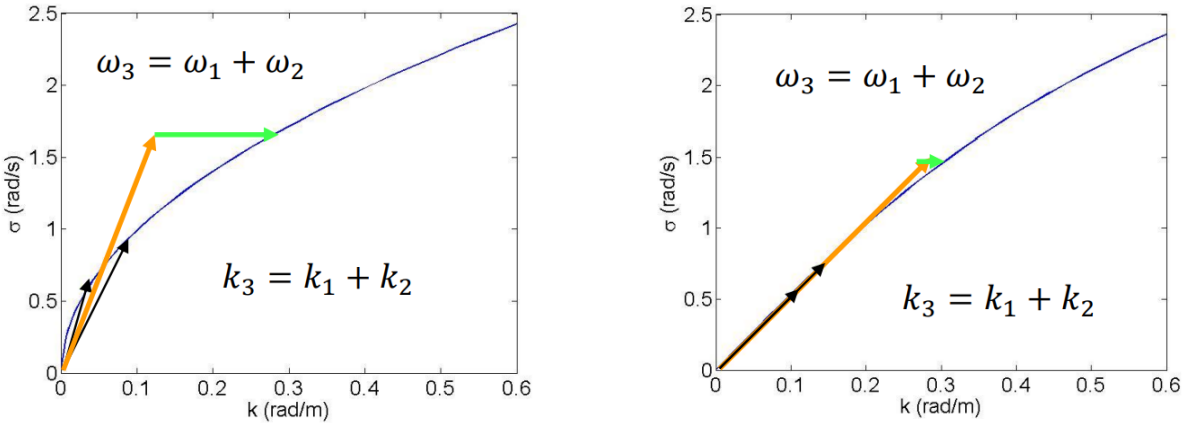

(a) Deep water conditions, resulting in a large mismatch.

(b) Shallow water conditions, resulting in a small mismatch.

Figure 2.9: Comparison of the resonance condition for triad wave-wave interactions between shallow and deep water. The orange line shows the third wave for which $\omega_3 = \omega_1 + \omega_2$ and $k_3 = k_1 + k_2$, the black line corresponds to the dispersion relationship, and the green arrow indicates the mismatch. Obtained from Tissier & Reniers (2021).

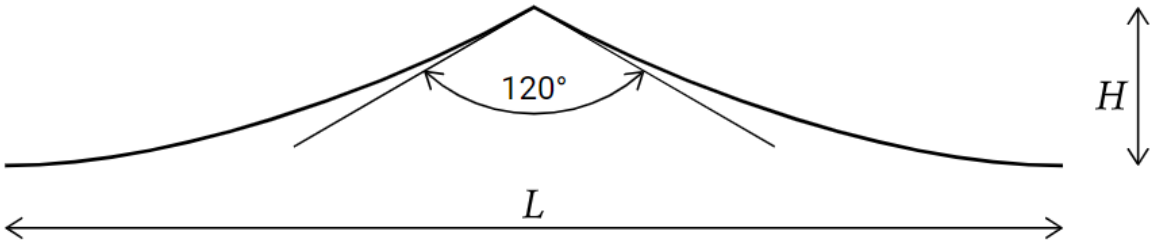

Figure 2.10: The maximum crest angle of 120 degrees for a stable wave in deep and shallow water. Obtained from Bosboom & Stive (2022).

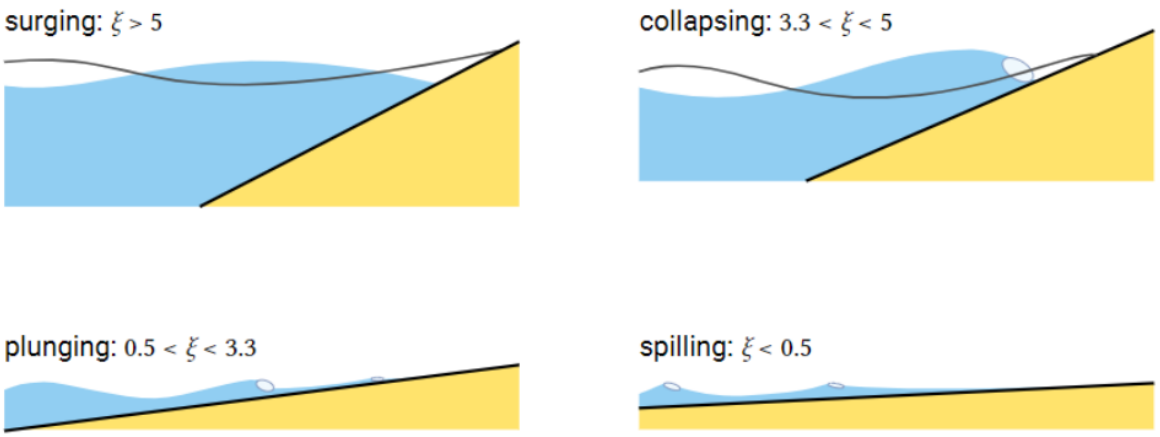

Figure 2.11: Different breaker types for waves approaching a beach, defined by the Iribarren parameter (equation 2.45). Obtained from Bosboom & Stive (2022).

3

The SWAN model

In the previous chapter, the principals of wave modelling have been treated with a special emphasis on modelling nonlinear effects such as triad wave-wave interactions and depth-induced wave breaking. These descriptions provide the theoretical background forming the basis of the spectral wave model SWAN. SWAN (Simulating WAves Nearshore) is a 3rd generation wave model, which means that the wave spectrum is free to develop at any point. As a result, the source terms describe the spectrum and its shape is not bounded a priori (Holthuijsen, 2007). Therefore, a good understanding of the individual source terms is important in assessing the main question of this investigation.

In this chapter, the governing equation for SWAN will be provided and the formulation of the source terms is explained. Furthermore, the basic performance of SWAN is addressed based on academic literature and performance reports.

3.1. Governing equation

SWAN is able to model wave-current interactions by means of the two-dimensional action balance, described by equation 3.1. This balance forms the basis of SWAN and is based on the spectral modelling approach described in section 2.2. The action density spectrum $N(\sigma)$ is an extension of the energy density spectrum $E(f)$, where the absolute radian frequency ω is replaced by the relative radian frequency σ in the linear wave equations (see also section 2.1.2) by means of $\sigma = \omega - \vec{k}\cdot\vec{U}$, where $\vec{k}$ and $\vec{U}$ denote the two-dimensional wave number and velocity vector. Through this transformation, SWAN is able to take into account effects produced by the presence of an ambient current, which are refraction, energy bunching and frequency-shifting (Holthuijsen, 2007).

The action balance (equation 3.1) consists of several terms which describe the generation, dissipation and propagation of wave action $N(t,\vec{x},\sigma,\theta)$ for a given point in geographical space $(x,y) = \vec{x}$. The terms on the left hand side describe 1) the rate of change of N in time, 2) the propagation of action in geographical space, including shoaling, 3) radian frequency shifting effects, and 4) depth-induced and current-induced refraction. The right hand term describes 5) the total source term which includes terms for energy input and dissipation, but also the terms describing the redistribution of energy between frequencies.

$$\underbrace{\frac{\partial N}{\partial t}}_{1} + \underbrace{\nabla_{\vec{x}}\cdot\left[(\vec{c}_g + \vec{U})N\right]}_{2} + \underbrace{\frac{\partial c_\sigma N}{\partial \sigma}}_{3} + \underbrace{\frac{\partial c_\theta N}{\partial \theta}}_{4} = \underbrace{\frac{S_{tot}}{\sigma}}_{5} \tag{3.1}$$

In this study, the SWAN model is used for one dimension in stationary mode (see section 4.2 for clarification), which simplifies the action balance. As a result, no rate of change in time is considered, the refraction term disappears and the geographical space simplifies to $(x,y) \rightarrow (x)$. Furthermore, no ambient current is included, which reduces the action balance $N(\sigma)$ to the energy balance $E(f)$. As a result, the energy balance consists of the balancing of two terms: the propagation of wave energy in x-direction and the total source term:

$$\frac{\partial c_g E}{\partial x} = S_{tot} \tag{3.2}$$

Closer investigation of equation 3.2 produces insights in the importance of the most term describing the spatial evolution of the energy-density spectrum in this idealized case: the sum of the source terms. The energy spectrum is changed by the source term while being convected by the group velocity c_g which, as a result of dispersion for high values of kd, may vary between wave components as $c_g = c_g(k)$ (see equation 2.25).

The total source term (equation 3.3) consists of six components, which are the deep water source terms: energy input by the wind (S_{wind}), energy dissipation due to white-capping (S_{wc}), quadruplet wave-wave interactions (S_{nl4}); and shallow water source terms: bottom friction (S_{fric}), depth-induced wave-breaking (S_{br}), and energy redistribution by the non-linear triads (S_{nl3}). An elaboration on the calibration of these source terms is given in the following sections.

$$S_{tot} = \underbrace{S_{wind} + S_{wc} + S_{nl4}}_{\text{deep water}} + \underbrace{S_{fric} + S_{br} + S_{nl3}}_{\text{shallow water}} \tag{3.3}$$

3.2. Deep water source terms

The deep water source terms consist of the wind input term, dissipation through white-capping and nonlinear quadruplet wave-wave interactions. In this section, a brief description of the formulation of each source term in SWAN will be presented. Although the name may suggest that these source terms only exist in deep water, they are also present in shallow water. They can even increase as shallow water effects: reduce the phase velocity resulting in a larger wind input term; increase possible quadruplet configurations, thus increasing wave-wave interactions; and increase the wave steepness, which enhances white-capping.

3.2.1. Wind input

The wind speed input in SWAN is defined as the wind speed at 10 metres above the water level U_{10}. This is then converted to the friction velocity u_* through $u_*^2 = C_D U_{10}^2$, where the wind drag coefficient C_D is obtained from Zijlema et al. (2012):

$$C_D = \left(0.55 + 2.97\bar{U} - 1.49\bar{U}^2\right) \times 10^{-3} \quad \text{where} \quad \bar{U} = U_{10}/31.5\ \text{m/s} \tag{3.4}$$

Wave generation consists of an initial linear wave growth term $S_{in,1} = \alpha$, constant in time (Phillips, 1957), and a positive feedback mechanism of exponential wave growth $S_{in,2} = \beta E(f)$ (Miles, 1957) resulting in the formulation equation 3.5. By default, SWAN uses the empirical expressions of Komen et al. (1984) to describe the positive feedback mechanism and included no linear growth ($\alpha = 0$).

$$S_{in} = \alpha + \beta E(f) \quad \text{with} \quad \alpha = 0 \quad \text{and} \quad \beta = \max\left[0, 0.25\frac{\rho_{air}}{\rho_{water}}\left(28\frac{U_*}{c}\cos(\theta - \theta_{wind}) - 1\right)\right]\sigma \tag{3.5}$$

3.2.2. White-capping

White-capping is represented in SWAN by the pulse-based model of K. Hasselmann (1974):

$$S_{wc} = -\mu k E(f) \quad \text{where} \quad C_{wc}\left((1-n) + n\frac{k}{\tilde{k}}\right)\left(\frac{\tilde{s}}{\tilde{s}_{PM}}\right)^p \frac{\tilde{\sigma}}{\tilde{k}} \tag{3.6}$$

C_{wc}, p and n are tunable coefficients, by default set to the values of Komen et al. (1984). Furthermore, $\tilde{\sigma}$ and $\tilde{k}$ denote the mean frequency and wave number, and the relative steepness of the waves is included through $\tilde{s}/\tilde{s}_{PM}$, where $\tilde{s} = \tilde{k}\sqrt{m_0}$ and $\tilde{s}_{PM}$ is the steepness of the Pierson-Moskowitz spectrum.

3.2.3. Quadruplet wave-wave interactions

Even though a comprehensive mathematical formulation of the quadruplet wave-wave interaction can be described (see also section 2.3.3), its calculation will be to extensive for practical use. Therefore, the discrete-interaction approximation (DIA) of S. Hasselmann et al. (1985). For this approach, two configuration of quadruplets are considered with the following frequencies (with $\lambda = 0.25$):

$$\begin{aligned} \sigma_1 &= \sigma_2 = \sigma \\ \sigma_3 &= \sigma(1+\lambda) = \sigma^+ \\ \sigma_4 &= \sigma(1-\lambda) = \sigma^- \end{aligned} \tag{3.7}$$

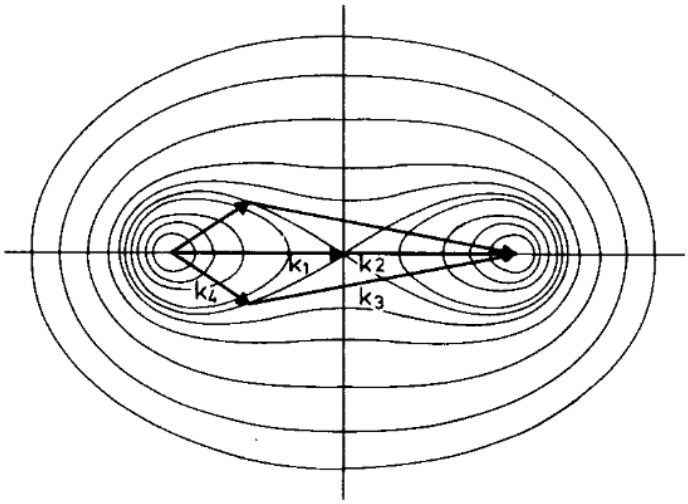

Figure 3.1: Two sets of quadruplets with $\theta_1 = -11.5°$ and $\theta_2 = 33.6°$. Obtained from S. Hasselmann et al. (1985).

In order to satisfy resonance conditions, the wave numbers must have a certain orientation, as shown in figure 3.1. The first quadruplet has wave-number vectors with angles $\theta_1 = -11.5°$ and $\theta_2 = 33.6°$, and the second quadruplet is identical but mirrored. The corresponding quadruplet source term S_{nl4} consists of the sum of both sets of quadruplets $(S^{*}_{nl4} + S^{**}_{nl4})$. For finite depth, the source term is multiplied with a scaling factor R (WAMDI Group, 1988):

$$R\left(k_{\mathrm{p}}d\right) = 1 + \frac{C_{sh1}}{k_p d}\left(1 - C_{\mathrm{sh2}}k_{\mathrm{p}}d\right)e^{C_{\mathrm{sh}}3k_{\mathrm{p}}d} \tag{3.8}$$

In this equation, k_p denotes the peak wave number and C_{sh1}, C_{sh2} and C_{sh3} are tunable coefficients for the shallow water effects.

3.3. Shallow water source terms

Waves travelling in shallow coastal waters experience different effects compared to deep oceanic waters. The deep water source terms tend to intensity, but simultaneously shallow water source terms start becoming active, such as the triad wave-wave interactions, dissipation due to wave breaking and the effects of bottom friction Holthuijsen (2007). Therefore, these source terms need to be included when modelling depth-limited situations and are thus included in this investigation.

3.3.1. Triad wave-wave interactions

Analogously to the quadruplet wave-wave interactions, the triad wave-wave interactions are the result of resonance between wave components in shallow water. SWAN offers three options to model triad wave-wave interactions: the LTA model, the SPB model and the CCA model.

As mentioned in section 2.3.3, the energy redistribution of the triads tends to concentrate round the harmonics of the peak frequency. This observation forms the basis of the Lumped Triad Approximation LTA) of Eldeberky & Battjes (1995) which only takes into account self-self interaction in the wave field, thus resulting in high computational efficiency. For the LTA model, the source terms consists of two terms: the increase of energy due to transfer from lower frequencies, and the decrease of energy as a result of energy transfer to higher frequencies:

$$S_{nl3}(f) = S^{+}_{nl3}(f) + S^{-}_{nl3}(f) \tag{3.9}$$

The first term adds energy to a frequency f from half its frequency $f/2$:

$$S^{+}_{nl3}(f) = \alpha_{EB}2\pi f^2 c c_g |\sin\beta_{peak}| \left[E^2(f/2) - 2E(f,\theta/2)E(f)\right] \tag{3.10}$$

The second term removes energy to twice its frequency $2f$ and is based on equation 3.10:

$$S^{-}_{nl3}(f,\theta) = -2S^{+}_{nl3}(2f,\theta) \tag{3.11}$$

These energy transfers depend on a tunable coefficient α_{EB}, the wave celerity c, group velocity c_g, the energy density spectrum E and the biphase β using the approximation in equation 2.40. The interaction coefficient (Madsen & Sorensen, 1993) is described by:

$$J = \frac{k_{\sigma/2}^2 \left(gd + 2c_{\sigma/2}^2\right)}{k_\sigma d \left(gd + \frac{2}{15} g d^3 k_\sigma^2 - \frac{2}{5}\sigma^2 d^2\right)} \tag{3.12}$$

Alternatively, Becq-Girard et al. (1999) have presented a model called Stochastic Parametric model based on Boussinesq equations (SPB). It is based on the closure relation of Holloway (1980) to calculate the bispectrum instead of using the parameterization using the Ursell number of the LTA model (Salmon, 2016), and offers the advantage of being fully directional compared to the uni-directional LTA model (Becq-Girard et al., 1999). The SPB model is not restricted to self-self interactions and thus redistributed the wave energy over a wider range of frequencies. Although the SPB model shows better performances than the LTA model (Becq-Girard et al., 1999; Salmon, 2016; Cavaleri et al., 2018), it has not been validated as extensively (Groeneweg & Gautier, 2020; Oosterlo, 2021). An example of improved performance for breaking waves is shown in figure 3.2.

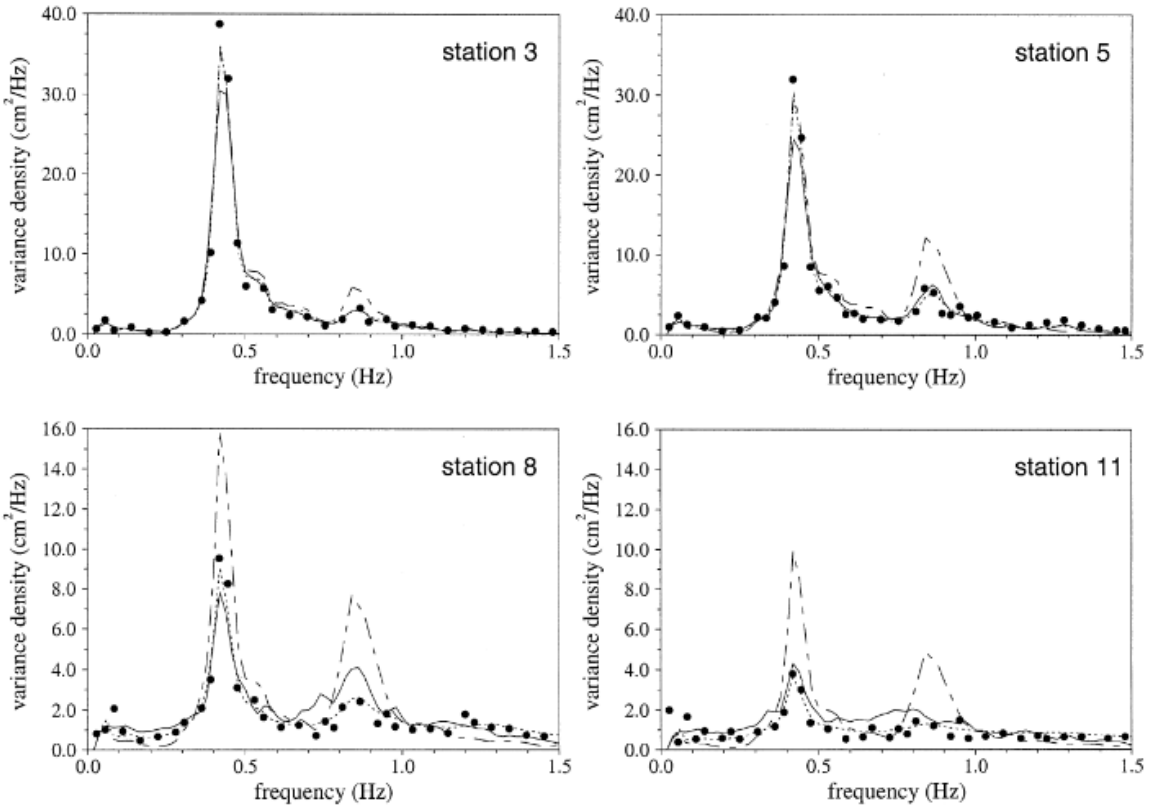

Figure 3.2: Spatial evolution of variance density spectra for breaking waves in a flume at the Laboratoire National d'Hydraulique in experiments by Becq-Girard et al. (1999). Breaking occurs past station 5. Comparison between measurements (circles), a deterministic model (solid line), the LTA model (dot-dashed line) and the SPB model (dotted line). Obtained from Becq-Girard et al. (1999).

The third model implemented in SWAN is the Consistent Collinear Approximation (CCA) of the LTA model (Salmon et al., 2016; Salmon, 2016). It has been proven by Salmon (2016) that the formulation of the LTA and SPB model introduces a strong dependency on the directional aperture, which can produce unbounded results for $\Delta\theta \rightarrow 0$, resulting in an unrealistic amplification of energy transfers, as shown in figure 3.3. Therefore, Salmon (2016) has derived a consisent formulation for the LTA model and SPB model, of which the first is implemented in SWAN as the CCA model.

3.3.2. Depth-induced wave breaking

When waves enter shallow water, they break and dissipate energy through a roller that is formed at the front of the wave crest. In SWAN, dissipation as a result of depth-induced wave breaking is modelled analogously to a

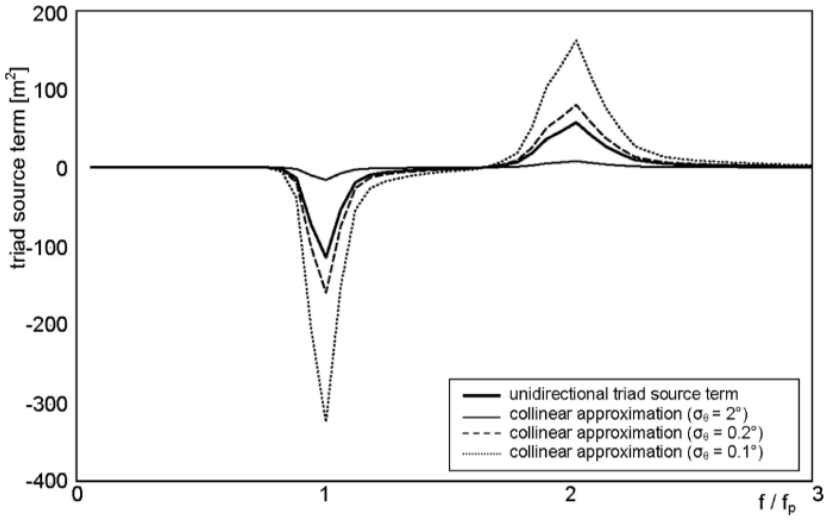

Figure 3.3: Energy transfers due to triad wave-wave interactions modelled by the LTA approach. In theory, the original collinear approximations should approach the unidirectional triad source term (thick black line). Obtained from Salmon et al. (2016).

bore (Stoker, 1957) as described by Battjes & Janssen (1978). Following they formulation, the total dissipation is presented in equation 3.13, where α is a proportionality coefficient, Q_b describes the fraction of breaking waves and $\bar{f}$ is the mean frequency of the spectrum.

$$D_{tot} = -\frac{1}{4}\alpha Q_b \bar{f} H_{breaking}^2 \tag{3.13}$$

Following this approach, two formulations must be derived: one for Q_b and one for $H_{breaking}$. By default, SWAN uses the equations derived by Battjes & Janssen (1978), hereafter called the BJ78-model. In this model, the maximum wave height $H_{breaking}$ is determined by the modified Miche-expression (Miche, 1944; Van der Westhuysen, 2010b):

$$H_{breaking} = 0.88 k_p^{-1} \tanh\left(\gamma k_p d / 0.88\right) \tag{3.14}$$

, which simplifies to $H_{breaking} = \gamma d$ for $k_p d \to 0$ in shallow water. While Battjes & Janssen propose a limit for the maximum wave height based on a constant breaking parameter $\gamma_{BJ} = 0.8$, SWAN uses a default value of $\gamma = 0.78$ which is an average found by Battjes & Stive based on an analysis of numerous field and laboratory experiments. However, several studies (Vink, 2001; Van der Westhuysen, 2009, 2010a; Salmon, 2016; Menéndez & Norscini, 1982) indicate that using a constant γ_{BJ} neglects important local processes, such as local wave steepness (Vink, 2001), nonlinearities (Van der Westhuysen, 2009, 2010a) and bottom slope and wave number (Ruessink et al., 2003; Salmon, 2016). Furthermore, in the case of wave growth conditions with depth-limited conditions (such as a horizontal bed in shallow water), it is found that SWAN, using the BJ78-model, tends to underestimate wave heights and periods (Van der Westhuysen, 2009, 2010a; Van Dongeren et al., 2011).

The fraction of breaking waves for SWAN is obtained by assuming that all waves break for which $H > H_{breaking}$ and that this process can be described using a Raileygh distribution. This results in the following formulation of the fraction of breaking waves (Battjes & Janssen, 1978):

$$\frac{1 - Q_b}{\ln(Q_b)} = -\left(\frac{H_{rms}}{H_{breaking}}\right)^2 \tag{3.15}$$

SWAN offers the option between the BJ78-model using a custom constant value for γ_{BJ}, and an alternative formulation proposed by Salmon (2016): the $\beta - kd$-model. For this formulation, the where the wave breaking parameter is a function of the bottom slope and the normalized wave number (equation 3.16). It contains three tuning parameters (a_1, a_2 and a_3), and is still compatible with formulations used in the BJ78-model.

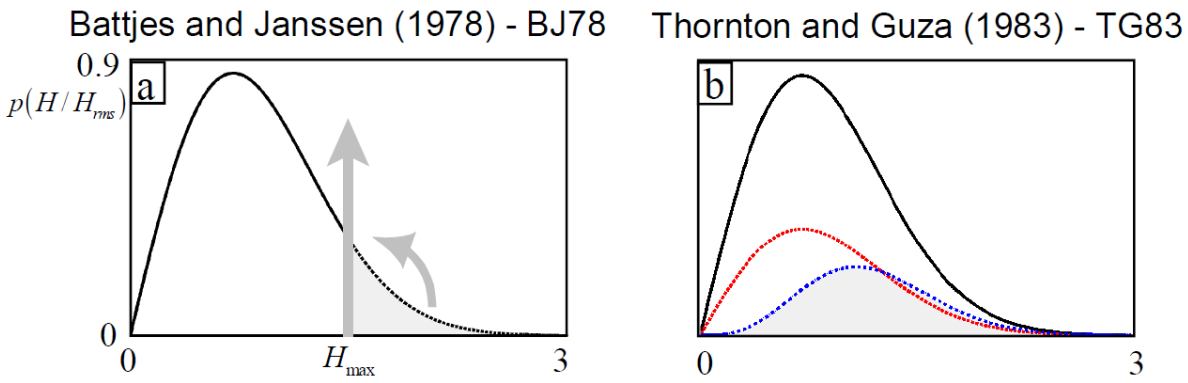

Figure 3.4: Comparison between the BJ78-model and TG83-model, adapted from Salmon (2016). The BJ78-model assumes that all waves for $H > H_{max}$ break based on the Raileygh distribution. The TG83-model assumes that all waves can break, first scaling down the Raileygh distribution (red line) and then skewing the distribution (blue line).

This results in the following formulation:

$$\gamma_{\beta-kd} = \gamma_1(\beta) / \tanh\left[\gamma_1(\beta)/\gamma_2(\tilde{k}d)\right] \tag{3.16}$$

for which:

$$\gamma_1(\beta) = \gamma_0 + a_1 \tan\beta \geq 0 \quad \text{and} \quad \gamma_2(\tilde{k}d) = a_2 + a_3 \tilde{k}d \geq 0 \tag{3.17}$$

Alternatively, Thornton & Guza (1983) propose a probabilistic description of wave breaking where each wave has a probability to break, abbreviated as the TG83-model. They use the Raileygh distribution as the basis, and apply a weighting function $W = W(H)$ that scales the distribution and skews it towards larger waves (as illustrated in figure 3.4):

$$Q_b = W(H) = \underbrace{\left(\frac{H_{rms}}{\gamma_{TG} d}\right)^n}_{\text{scaling}} \underbrace{\left(1 - \exp\left(-\left(\frac{H}{\gamma_{TG} d}\right)^2\right)\right)}_{\text{skewing}} \tag{3.18}$$

In this equation, n is a calibration parameter and γ_{TG} is an alternative breaking parameter. This formulation is not implemented in the current version of SWAN.

Furthermore, the reports of Deltares (Groeneweg & Gautier, 2020; Gautier, 2020; Groeneweg, 2021; Oosterlo, 2021) describe a version of SWAN in which the breaking formulation of Van der Westhuysen (2010b) is adapted. Similarly to Thornton & Guza (1983), it is assumed that all waves have a probability to break and a weighting function is introduced. However, it is based on the assumption that nonlinearities in the wave field affect wave breaking. Thus, the weighting function becomes a function of the biphase: $W = W(\beta)$ (not to be confused with the bottom slope β of the $\beta - kd$-model):

$$Q_b = W(\beta) = \left(\frac{\beta}{\beta_{\text{rcf}}}\right)^n \tag{3.19}$$

3.3.3. Bottom friction

The final shallow water source term described by SWAN is bottom friction. By default, this term is described by the empirical JONSWAP equation (K. Hasselmann et al., 1973; Holthuijsen, 2007):

$$S_b(f) = -\chi \frac{k^2 E(f}{(2\pi f)^2 \cosh^2 kd} \tag{3.20}$$

The bottom friction term thus depends on the water depth d, the wave number k and the bottom friction coefficient χ. Initially, it was thought that for swell wave conditions $\chi = 0.038\ \text{m}^2\text{s}^{-3}$ had to be used (K. Hasselmann et al., 1973) and $\chi = 0.067\ \text{m}^2\text{s}^{-3}$ for fully developed wind waves (Bouws & Komen, 1983). However, it has been shown by Vledder et al. (2012) that a value of $\chi = 0.038\ \text{m}^2\text{s}^{-3}$ for both swell and wind wave conditions is more suitable, especially when using the current wind drag formulation in SWAN (see also section 3.2.1) instead of the previous formulation derived by Wu (1982) (Zijlema et al., 2012).

4

Methodology

In order to investigate the source behind the growing low frequency peaks, several SWAN runs will be performed using the mentioned simplifications and taking the relevant variables into account. Similarly to the Deltares report (Groeneweg, 2021), a one-dimensional transect with a length of 30 kilometers will be modelled (representing the simplified Markermeer) with a constant wind speed and flat bottom along the whole transect. Furthermore, the source term formulations and their parameters are described, highlighting the parameters which will be investigated.

4.1. Case study description

Wave generation modelling is only relevant for a number of lakes in the Netherlands as wave growth is limited for small lakes due to the short fetch. For these lakes, RWS uses SWAN-models to predict wave heights Gautier (2020). These are the following lakes: It should be noted that these lakes are all relatively shallow, which

	IJssel-meer	Marker-meer	Gooi-meer	Eem-meer	Ketel-meer	Vosse-meer	Zwarte Meer
Depth [m]	3.0 to 3.5	2.8 to 5.8	2.6	2.6	2.7 to 4.2	2.6	3.0

Table 4.1: Revelant lakes and their water depths with respect to NAP.

implies that shallow-water effects should be considered, for example the triad wave-wave interactions. The calibration of these triads formed the subject of a Deltares study Groeneweg (2021), in which inconsistencies appeared in the energy spectrum of the Markermeer for large wind speeds (figure 4.1). A second peak starts to grow in the low-frequency part of the spectrum without clear cause, although it is suggested that it may be linked to the triad source term of SWAN.

4.2. Model schematization

In order to isolate the processes governing the emergence of the low-frequency peak, the case study described in section 4.1 will be simplified. Similarly to Groeneweg (2021), the Markermeer will be modelled as a one-dimensional transect with $L = 30km$. Although the first observations of the second low frequency peak were obtained in 2D models, they have also been reproduced in a 1D model (Groeneweg, 2021). Reducing the model from two to one dimension removes the effects of diffraction and refraction. Likewise, a one-dimensional model aligns all source terms with the spatial direction and removes the influence of boundary conditions on the sides of the transect. Furthermore, computations take considerably less time in comparison to a two-dimensional model, which is convenient due to the limited time available during this study.

Besides reducing the case study to a one-dimensional model, some simplifications are applied to the transect geometry. A constant water depth (flat bottom) is assumed, which removes the effects of shoaling on the energy density spectrum and simplifies the evaluation of other source terms as variations in these terms will only depend on changes in the energy density spectrum itself and not the water depth. Because the water level would become sloped in reality due to the wind, choosing a constant water level will lead to conservative

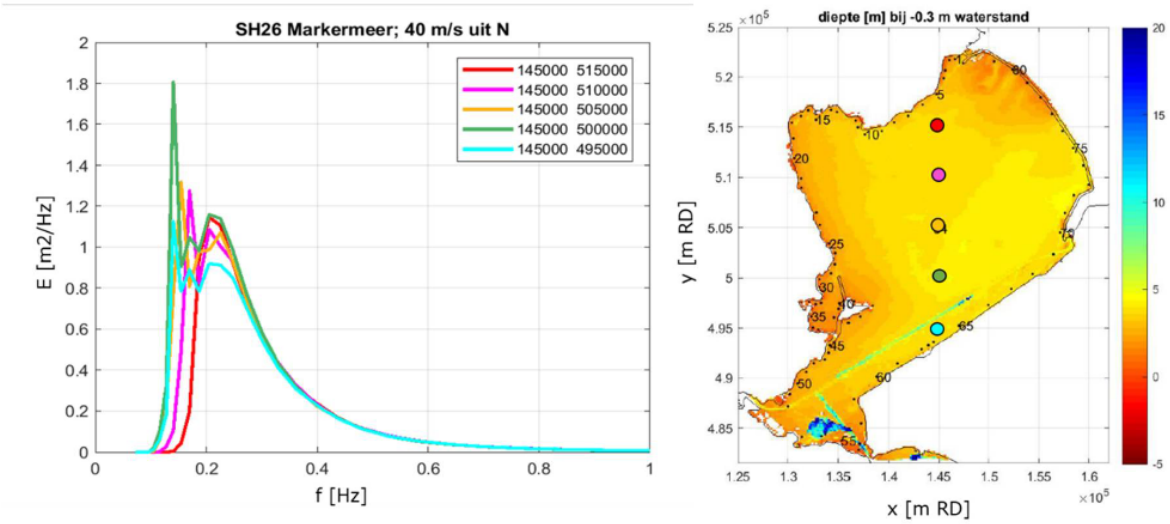

Figure 4.1: SWAN results for the Markermeer using $U_{10} = 40 m/s$, showing inconsistent behaviour in the low frequency region of the spectrum. Groeneweg (2021)

results. However, in practice this difference is negligible (Groeneweg, 2021). In order to represent the case study, a depth of $d = 2.5m$ is considered. Additionally, no downstream boundary condition will be imposed and the whole transect is subjected to a constant wind speed. The model will be run in stationary mode in order to remove time-dependent effects, so only the final, stationary result will be considered. This simplification is valid when the time scale of variations in the boundary conditions is much larger than the residence time of the waves (Holthuijsen et al., 1996), which is especially true for the high and constant wind speed in this investigation. Finally, no currents will be considered in this investigation in order to focus solely on the evolution of the energy spectrum due to wave action. The result is provided in figure 4.2.

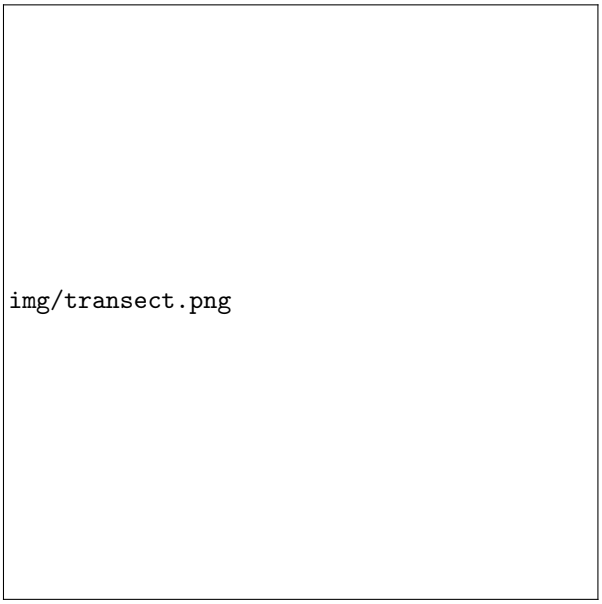

Figure 4.2: Schematized model with flat bottom and constant wind speed.

4.3. Parameter selection of the source terms

The focus of this study is on the shallow source terms and their interactions. Therefore, most model parameters are fixed and correspond to the default SWAN settings. The deep water source terms remain fixed as well as

the bottom friction source term with the parameters described in table 4.2.

Source term	Formulation	Parameters (default)
Wind input	`GEN3 KOMEN` (Komen et al., 1984)	`[cds2] = 2.36e-5 , [stpm] = 3.02e-3`
White-capping	`WCAP KOMEN` (Komen et al., 1984)	`[cds2] = 2.36e-5 , [stpm] = 3.02e-3 , [powst] = 2 , [delta] = 2 , [powk] = 1`
Quadruplets	`QUAD` (S. Hasselmann et al., 1985) with explicit DIA computation `[iquad] = 2`	`[lambda] = 0.25 , [Cnl4] = 3e07 , [Csh1] = 5.5 , [Csh2] = 0.833333 , [Csh3] = -1.25`
Bottom friction	`FRICTION JONSWAP` (K. Hasselmann et al., 1973)	`[cfjon] = 0.038`

Table 4.2: Chosen formulations for the fixed source terms with their default parameters for the SWAN model.

The parameter selection for depth induced wave breaking and triad wave-wave interactions differs from the other source terms. As it is suspected that these shallow water source terms create the secondary spectral peak in shallow lakes, several formulations and parameters will be varied and compared.

Modelling of the triads consists of three options: the LTA model (`[itriad] = 1`), SPB model (`[itriad] = 2`) and CCA model (`[itriad] = 8`) (see also section 3.3.1). In theory, Salmon (2016) has proven that the LTA model is inconsistent and thus not suitable for modelling. However, its inconsistency is related to the directional width of the wave field in SWAN, and thus should not affect model results in one dimension as this would always result in an unidirectional source term. Still, this study will focus on the CCA model as the results obtained in one dimension should provide insights that would provide guidance in more complex modelling of two dimensional shallow lakes. Furthermore, the SPB model will only be considered briefly as its applicability has not been validated as much as the LTA model (and thus its CCA counterpart).

SWAN takes several parameters when modelling triad wave-wave interactions using the CCA approach:

- `[trfac]`: the proportionality coefficient, see α_{EB} in equation 3.10 (default: 0.05 for LTA and 0.8 for CCA)
- `[cutfr]`: the maximum frequency considered in the LTA computation (default: 2.5 Hz)
- `[urcrit]`: the critical Ursell number appearing in the expression for the biphase (default: 0.2)
- `[urslim]`: the lower threshold for Ursell number (default: 0.01)

Salmon (2016) explains that inconsistencies in triad modelling with the LTA approach have resulted in the use of lower proportionality coefficient in order to counteract these effects. In practice, the use of coefficients at least an order of magnitude smaller than those found in literature ensued. For example. Salmon (2016) showed that optimal values of $\alpha \approx 0.04$ were found for the LTA model while the CCA implementation resulted in $\alpha_{EB} = 0.52$, which is closer to the original $\alpha = 1$. Holthuijsen et al. (1999) used $\alpha_{EB} = 0.25$ in their original validation of SWAN using the LTA model, after comparing results for $0.125 \leq \alpha_{EB} \leq 0.5$, and Becq et al. (1998) investigated LTA performance using $\alpha_{EB} = 0.5$. On the other hand, Van der Westhuysen (2007) found with $\alpha_{EB} = 0.05$ an even lower optimal value for the proportionality coefficient of the LTA model, and also concluded that the triad source term was small as a result of this low coefficient compared to other triad models. Following these investigations, the proportionality factor of the triad source term `trfac` will be revisited in this investigation.

Depth-induced wave breaking in SWAN is modelled using the BJ78-model (see also section 3.3.2). Two approaches are possible: one with a constant breaking parameter `CONSTANT` and one with the $\beta - kd$-model `BKD`. The

BJ78-model can be calibrated by changing the breaking parameter γ and the proportionality factor α. However, as noted by Battjes & Stive (1985), both coefficients affect the total dissipation therefore resulting in effectively one degree of freedom. By setting $\alpha = 1$, a constraint is set and thus the breaking parameter becomes the degree of freedom.

Several values for the breaking parameter are suggested by academic literature. For example, Battjes & Janssen (1978) suggest $\gamma_{BJ} = 0.8$ based on the Miche breaking-criterion, and Nelson (1997) argues that $\gamma_{BJ} \leq 0.55$ for horizontal bottoms. Battjes & Stive (1985) analysed several laboratory and field experiments and derived an averaged value of $\gamma_{BJ} = 0.73$, which is currently the default value of SWAN. Similarly, Salmon (2016) derived a function for $\gamma_{\beta-kd}$ with the default parameters `[a1] = 7.59`, `[a2] = -8.06` and `[a3] = 8.09` with a reference value of `[gamma0] = 0.54` for horizontal slopes. In order to investigate the effects of the breaking source term in this investigation, the breaking parameter will be varied for the BJ78-model. For the $\beta - kd$-model, the parameter `[a3]` will be varied as it influences the effectiveness of the breaking criterion for young wind waves (high kd-value), and thus distinguishes between non-locally and locally generated waves (Salmon, 2016). Therefore, we are able to test whether varying this parameter will improve source term interactions along the whole spectrum. The summarized result for the parameters of the triad wave-wave interactions and depth-induced wave breaking is shown in table 4.3.

Source term	Formulation	Fixed parameters	Variable parameters

Triad wave-wave interactions	`TRIAD [itriad] = 8` (Salmon, 2016)	`[urcrit] = 0.2`
		`[cutfr] = 2.5`
		`[urslim] = 0.01`
			`[trfac]`

Depth-induced breaking	`BREAKING CONSTANT` (Battjes & Janssen, 1978)	`[alpha] = 1.0`	`[gamma]`

Depth-induced breaking	`BREAKING BKD` (Salmon, 2016)	`[alpha] = 1.0`
		`[gamma0] = 0.54`
		`[a1] = 7.59`
		`[a2] = -8.06`
			`[a3]`

Table 4.3: Fixed and variable parameters for the source terms of triad wave-wave interactions and depth-induced wave breaking for the SWAN model.

4.4. Resolution and numerical parameters

Following the setup of Groeneweg (2021), a spatial resolution is selected of $\Delta x = 30$ m, resulting in 1001 spatial grid points. The size of the lake is of order 30 km, so the selected grid size provides a fine spatial resolution and is in accordance with typical grid sizes for the surf zone (Holthuijsen, 2007). As SWAN will be used in stationary mode, no time step needs to be considered. In practice, the numerical solution must still converge which can be regarded as a time marching method (Zijlema & Van der Westhuysen, 2005), and frequency shifting may pose a limit on the grid sizes based on the CFL-criterion (Dietrich et al., 2013). Action limiters can improve convergence of model results and are therefore also applied in SWAN in the form of the action limiter, where it limits the maximum change the energy density per spectral bin for each iteration (The SWAN team, 2021). This maximum change is defined as:

$$\Delta N = \gamma \frac{\alpha_{\mathrm{PM}}}{2\sigma k^3 c_g} \tag{4.1}$$

, where γ denotes the limitation factor, k is the wave number and α_{PM} = 8.1 x 10-3 is the Phillips constant for a Pierson-Moskowitz spectrum. In SWAN, this limit has been set to 10% (Tolman, 1992). It has been shown by Ris et al. (1999) that limiter settings may affect SWAN results. Due to the many source terms interacting in the lake problem, we will consider whether tuning the limiter may improve model results.

The frequency bins of the spectrum are distributed logarithmically in SWAN, and its division is determined

by three elements: the minimum frequency f_{low}, the maximum frequency f_{high} and the number of spectral bins `msc`, as shown in equation 4.2.

$$\frac{\Delta f}{f} = -1 + \left(\frac{f_{high}}{f_{low}}\right)^{1/\texttt{msc}} \tag{4.2}$$

The frequency resolution $\Delta f / f$ is usually set to 0.1 as the DIA approximation of the quadruplets source term has been calibrated for this value (S. Hasselmann et al., 1985; Van der Westhuysen, 2007; The SWAN team, 2021). However, finer resolutions are often found in literature for the calibration of the triad source term , for example $\Delta f / f = 0.05$ by Salmon (2016), $\Delta f / f = 0.055$ by Bénit (2009) and $\Delta f / f = 0.07$ by Eldeberky & Battjes (1995). The source terms are confined to the spectral bins, which may affect their interactions. Therefore, the spectral resolution will be varied and investigated. Additionally, it is observed that the secondary low-frequency peak emerges near the lower frequency limit of 0.8 Hz, so the effect of lowering the frequency limit is also considered. However, such a lower limit should only affect model results when the bins are effectively used: no numerical improvement is obtained when the spectrum does not reach these lower frequencies (Tolman, 1992).

5

Results

5.1. Wind speed and water depth

As described in section 4.1, the case study is based on shallow lakes with relatively short fetch in the Netherlands. The total water depth depends on the water level which may vary due to hydrological conditions: a high water run-off due to large precipitation may result in an increase of the water level. Note that these lakes are not directly connected to the sea, therefore neglecting the influence of the tide on the water level.

Several water depths and wind speeds are compared with the objective of narrowing the selection of water depths and wind speeds used in this investigation. A range of d = 1.0, 2.5, 5.0 and 10.0 m and U_{10} = 10.0, 20.0 and 40.0 m/s is chosen to cover normal to extreme wind conditions for several types of shallow lakes. For these runs, the energy-density spectra at x = 30 are compared in order to identify the possible emergence of the second low-frequency peak (figure 5.1). The location is chosen at the end of the lake as an equilibrium between the energy source terms, and therefore a constant significant wave height H_{m0}, is found at the end of the fetch. Additionally, the relative significant wave height H_{m0}/d is compared along the fetch in order to whether shallow water effects are expected to be significant.

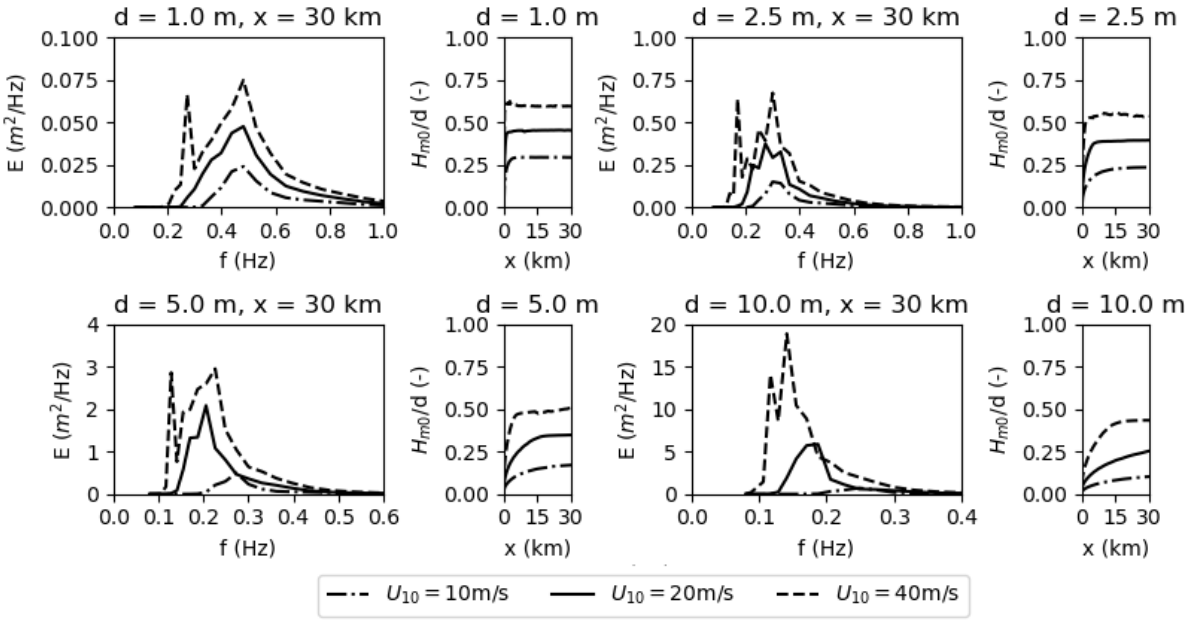

Figure 5.1: Energy density spectra and relative significant wave height for a range of wind speeds and water depths.

We observe that the low frequency peak occurs for all water depths at a wind speeds of U_{10} = 40 m/s, and does not occur for U_{10} = 10 m/s. For the intermediate wind speed of U_{10} = 20 m/s, the low frequency peak begins

to emerge as the water depth decreases and the relative significant wave height increases: a distinct second peak can be identified for d = 1.0 and 2.5 m. Even though smaller water depths results in a large decrease of wave energy, the relative significant wave height remains of the same order and thus shallow water effects appear to be significant for U_{10} = 20 and 40 m/s. We expect shallow water effects to be the strongest for the water depth of d = 1.0 m, as it contains the largest relative significant wave height. However, a water depth of d = 1.0 m is in practice very shallow, even compared to the shallow lakes shown in table 4.1, and wave energy remains very low as wave heights are limited due to the small water depth. As a result of this, a larger water depth of d = 2.5 m is chosen as a more practical water depth for the base case for this study using wind speeds of U_{10} = 20 and 40 m/s.

5.2. Proportionality coefficient trfac

The non linear wave-wave interactions of the triads are important for the redistribution of the wave energy in shallow water. These interactions are modelled using the CCA-method which includes a proportionality coefficient that can be varied in SWAN: `trfac`. For the CCA-method, the default setting is set to `trfac = 0.8`, which is based on calibration by Salmon (2016). As a result, the magnitude of this proportionality coefficient influences the effect of the triad source term on the energy balance of the wave field. However, changing `trfac` does not simply result in a linear scaling of the triads as the triad source term itself is non-linear and depends on the wave field which may be altered due to changes in the triads source term.

A range of factors is compared to the default setting in SWAN (`trfac = 0.8`), varying from `trfac = 0.05` (as proposed by Groeneweg & Gautier (2020)) to `0.4`. Figures 5.2a and 5.2b demonstrate the corresponding energy density spectra E at $x = 30$ km, and the ratio of the energy redistributed by the triads and by the quadruplets, which provides insight in the change of balance between these non-linear source terms. The

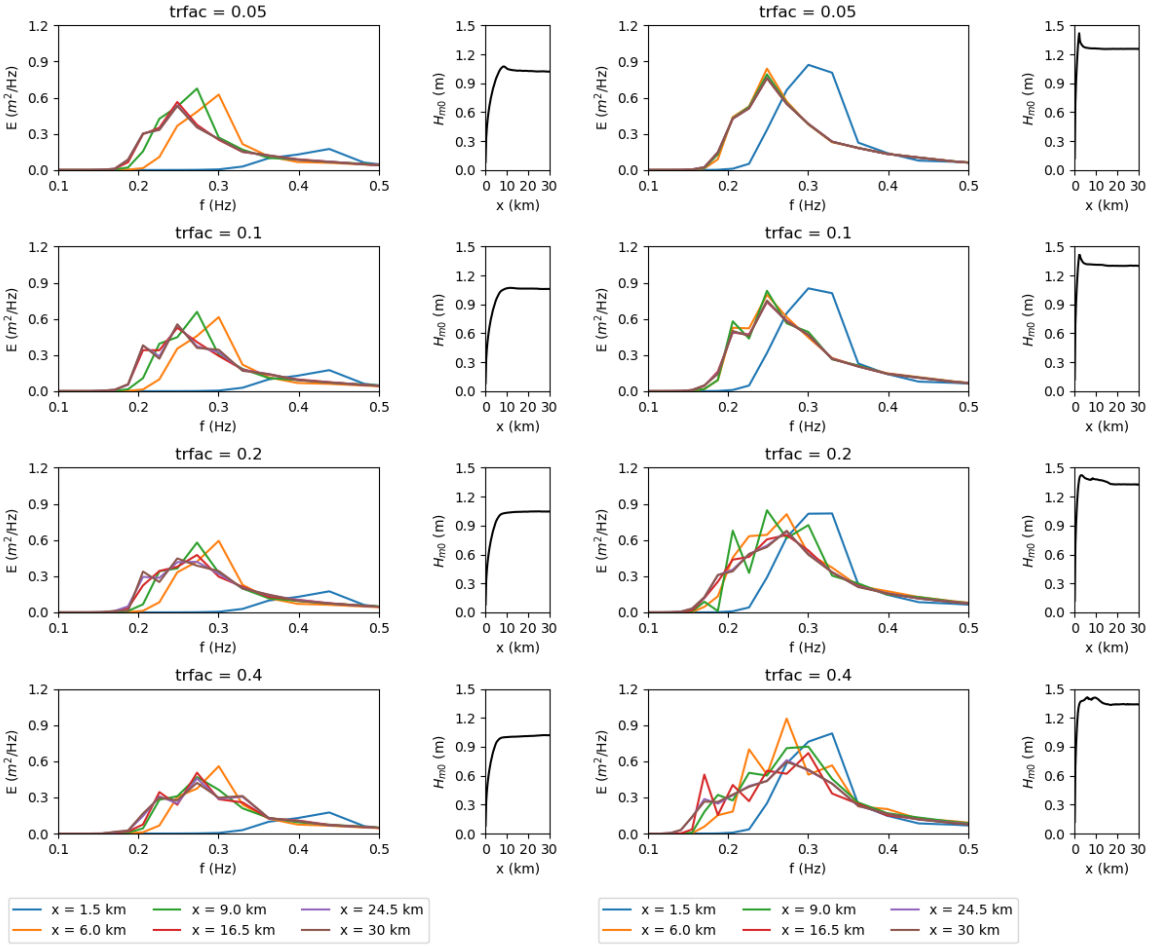

(a) Results for $U_{10} = 20$ m/s.

(b) Results for $U_{10} = 40$ m/s.

Figure 5.2: Energy density spectra at several locations for varying `[trfac]` using the $\beta - kd$-model.

results indicate that changing the proportionality coefficient affects the size of the low-frequency peak, as it becomes smaller as the proportionality coefficient decreases. Furthermore, a lower value for `trfac` results in a faster equilibrium state, and all results show an equilibrium state at $x = 30$ km. The effect of reducing `trfac` on the source terms is highlighted in figure 5.3. A lower proportionality coefficient results in a smoother shape of the nonlinear source terms and more balanced values for their sum. Theoretically, the non-linear energy transfers should not create or dissipate energy: $|\int(S_{red})df| = |\int(S_{nl3} + S_{nl4})df| = 0$. Therefore, a balanced sum for S_{red} with an integral close to zero is desirable. For `[trfac]=0.8`, wiggles are observed for the sum of the triad and quadruplet source term for frequencies near the secondary energy peak in the low frequency

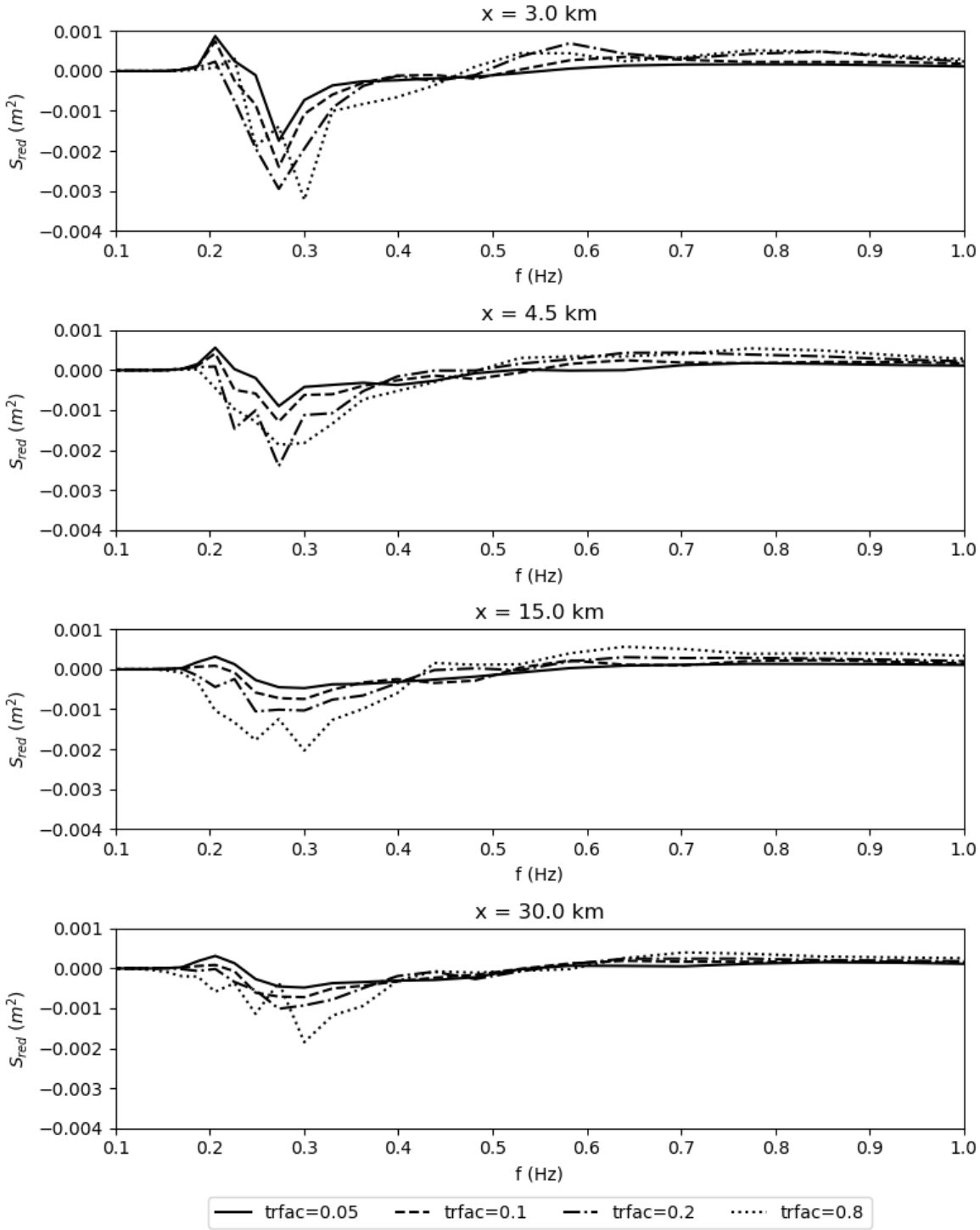

Figure 5.3: Sum of the nonlinear source terms S_{nl3} and S_{nl4} for varying `trfac` for U_{10} = 40 m/s at several locations.

tail.

This indicates that the transfer of energy to this location may be caused by the interactions between the triad and quadruplet source terms. The triad source term is responsible for energy redistribution from the peak frequency to higher harmonics. Thus, by increasing the proportionality factor of the triad source term one would expect less energy transfer to lower frequencies. In practice, the secondary peak emerges at

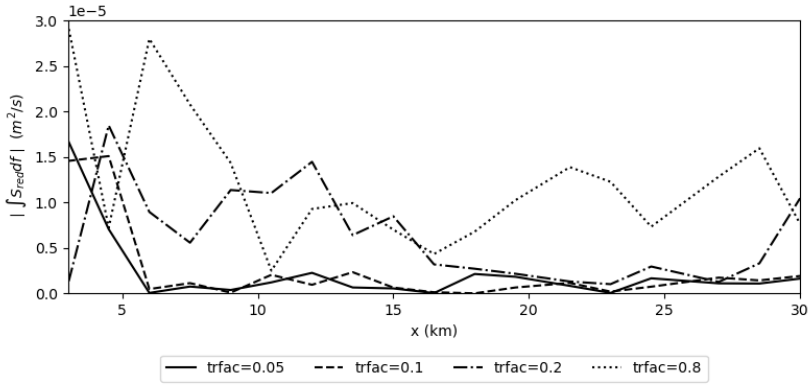

Figure 5.4: Integral of the sum of the nonlinear source terms S_{nl3} and S_{nl4} for varying `trfac` for U_{10} = 40 m/s. The first location (x = 0 m) has not been included as it produced large values for the integral for all `trfac`.

frequencies lower than the peak frequency and are therefore not directly affected by the triad source term. Observing the source terms shows that a slight mismatch exists between the shape and peak frequencies of S_{nl3} and S_{nl4}, which causes the redistribution of energy shown in figure 5.3. Lowering the proportionality factor for the triads primarily affects the triad source term around the peak frequency of the spectrum, and has less effect on the triad source term for lower frequencies, which remain small but non-zero. Even for `[trfac]=0.05`, a slight mismatch remains and can be observed.

As mentioned earlier, one would expect the integral of the triad and quadruplet wave terms over the frequency domain to equal zero. In practice, SWAN does not always satisfy this property due to approximation of the source terms and numerical errors like truncation and rounding errors. Figure 5.4 demonstrates this effect as $|\int(S_{red})df|$ describes the integral over the frequency domain for the sum of the nonlinear triad and quadruplets source terms using Simpson's rule. Still, we observe that the choice of `trfac` seems to affect this property of the balance between the source terms, as a lower proportionality coefficient results in net energy changes closer to zero.

Furthermore, the effect of `trfac` on the significant wave height H_{m0} can be observed in figures 5.2a and 5.2b, where lower values for the significant wave height are observed for decreasing `trfac`. This effect varies between the wind speeds U_{10} = 20 m/s and 40 m/s.

5.3. Variations in depth-induced wave breaking

The effect of varying the wave breaking parameter on the triads and the low-frequency energy peak has also been investigated. First, the BJ78-model has been used with breaking parameter values ranging from 0.54 to 1.0 in model runs (figures 5.5a and 5.5b), resulting in maximum wave heights varying from $H_{max} = \gamma d =$ 1.35 to 2.5 m for $d = 2.5$ m. Similar ranges of wave breaking parameters have been used in the investigations of Battjes & Stive (1985), where varying breaking parameters were obtained for specific wave-related conditions and bathymetries. The lower limit of $\gamma = 0.54$ is based on the work of Nelson (1997), who derived this limit for waves over (nearly) horizontal bottoms.

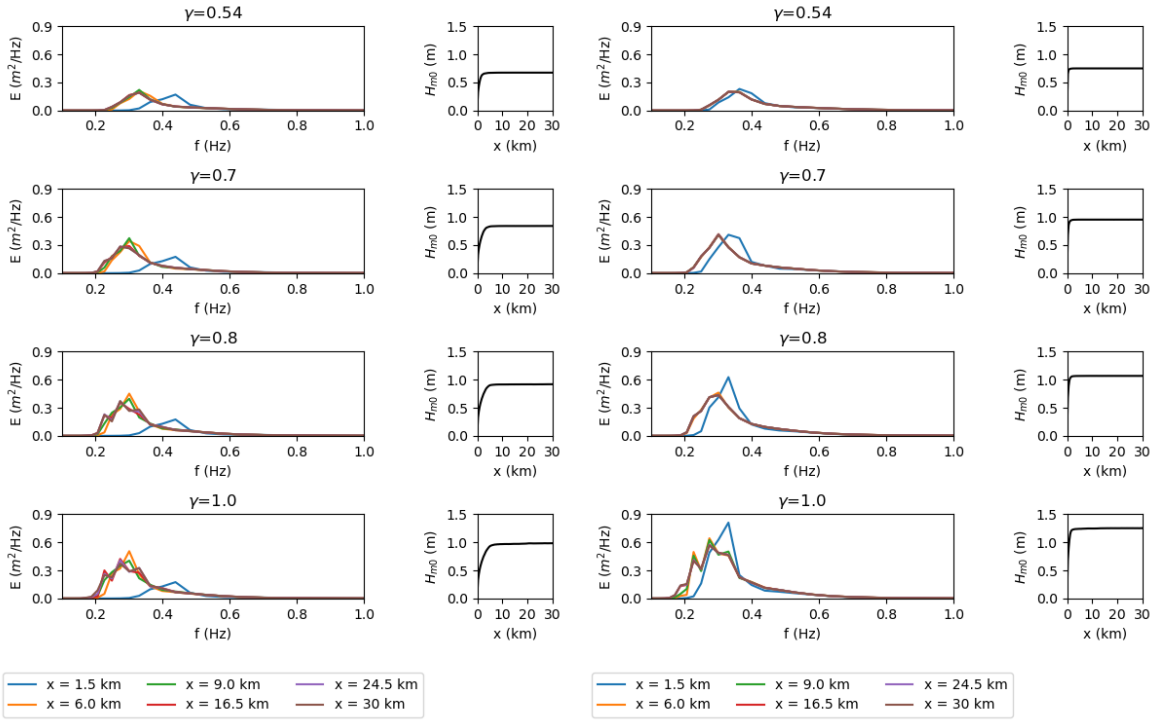

(a) Results for $U_{10} = 20$ m/s.

(b) Results for $U_{10} = 40$ m/s.

Figure 5.5: Energy density spectra at several locations for varying breaking parameters using the BJ78-model.

On first sight, it appears that using $\gamma \leq 0.7$ results in no secondary peaks in the energy density spectrum. However, this also reduces the significant wave height substantially, especially for higher wind speeds. Higher values for the breaking parameters result in increased wave energy, which is to be expected as larger wave heights are allowed, but introduce the secondary energy peak in the low frequency tail of the spectrum. Furthermore, a higher breaking parameter allows the wave spectrum to develop as less damping is introduced by limiting the maximum wave height. As a result, the significant wave height increases but the spectrum itself becomes less smooth.

For the $\beta - kd$-model, the breaking parameter becomes a function of kd, as illustrated in figure 5.7. The parameter `[a3]` can be used to vary the effect of wave breaking on younger waves in the spectrum (with higher kd), and several values for `[a3]` have been used to produce model results (figures 5.6a and 5.6b). These results show similarities with the previous results using $\gamma = 1.0$, which is to be expected: no depth-induced wave breaking occurs in the results of the first kilometers for both the BJ78-model (using a large breaking parameter) and the $\beta - kd$-model, so the spectra should be similar. When wave breaking becomes active, differences can be observed between spectra using varying values for `[a3]` for $U_{10} = 40$ m/s. Using values for `[a3]` produces smoother wave spectra and reduces the low frequency peak while maintaining a similar significant wave height when compared to other results.

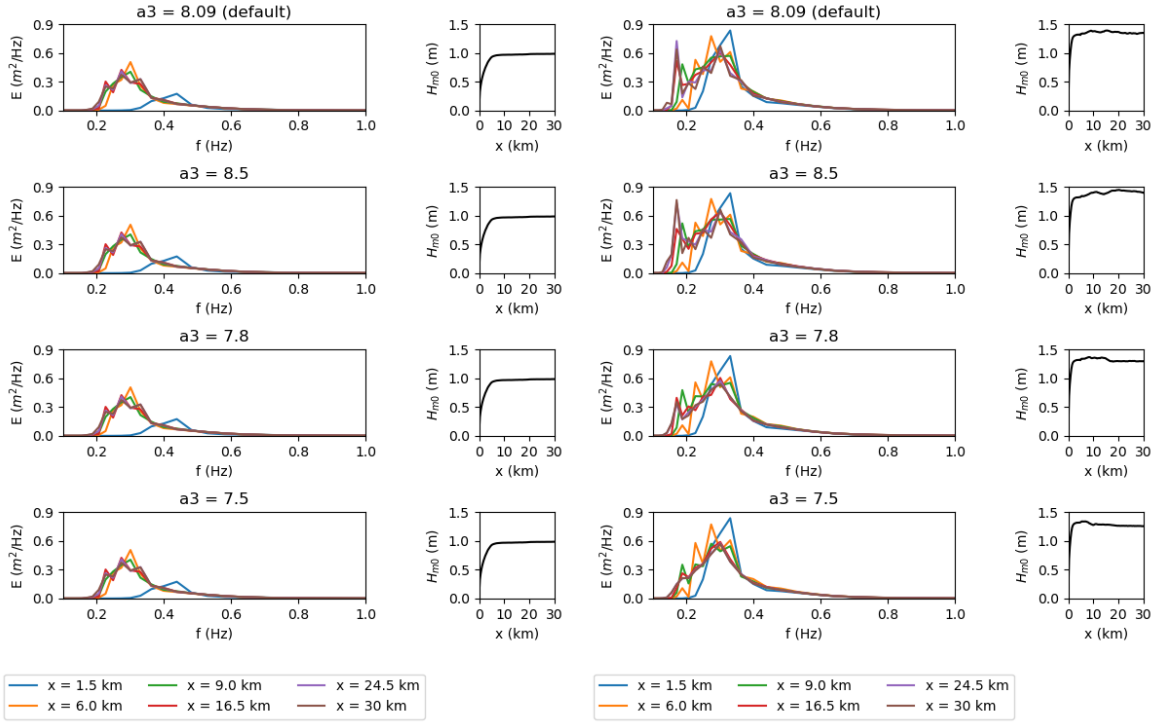

(a) Results for $U_{10} = 20$ m/s.

(b) Results for $U_{10} = 40$ m/s.

Figure 5.6: Energy density spectra at several locations for varying `[a3]` using the $\beta - kd$-model.

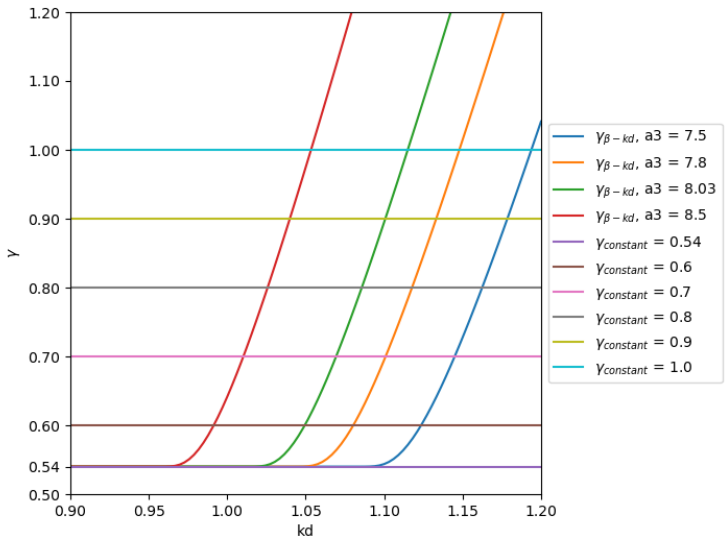

Figure 5.7: Graphical representation of the used breaking parameters and their dependencies on the relative water depth kd.

5.4. Frequency resolution msc

The 'spiky' shapes of the energy density spectra and source terms for the base case suggests that the frequency resolution may play a role in explaining the emergence of the additional low-frequency peak, as these spiky source terms may produce small peaks in the energy density spectrum that may amplify.

Generally, SWAN recommends the use of $\Delta f / f = 0.1$ as this resolution has been used for the DIA approximation of the quadruplet wave-wave interactions, and by default SWAN will determine `msc` based on $\Delta f / f = 0.1$ and a given f_{low} and f_{high}. For the base case, the frequency boundaries are set to $f_{low} = 0.08$ Hz and $f_{high} = 2.4$ Hz, resulting in `msc = 37`. In order to investigate the effect of varying the frequency resolutions, slight variations in `msc` are introduced at several locations (figure 5.8).

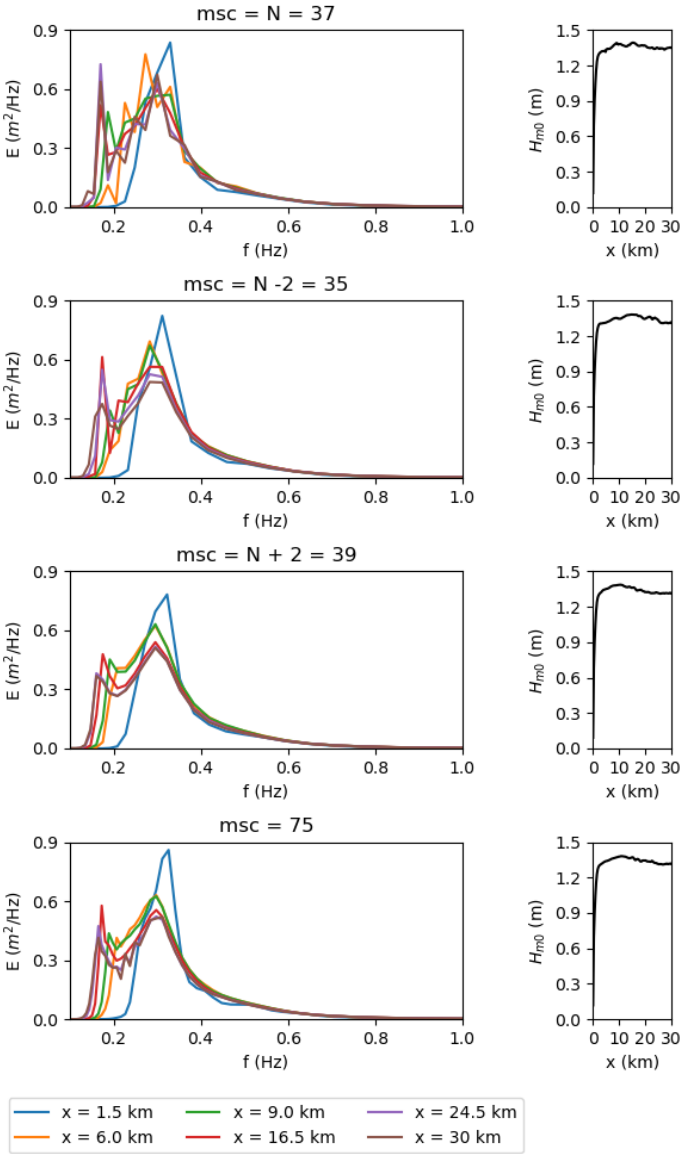

Figure 5.8: Energy density spectra for slight variations in spectral resolutions for $U_{10} = 40$ m/s.

The results in figure 5.8 indicate that changing the spectral resolution results in a smoother energy density spectrum while the secondary peak still remains. It is striking how adding or removing two grid points can change model results with such impact. Doubling the resolution (`msc = 75`) shows similar improvements compared to the default resolution used by SWAN. Still, a secondary peak at lower frequencies prevails. The

significant wave height remains similar as the shape of the spectrum is similar for all four spectral resolutions, thus resulting in approximately the same total wave energy. Closer comparison of the source terms for `msc = 37` and `msc = 39` (figure 5.9) reveals that the source terms themselves become smoother for a slight change in spectral resolution, with no clear wiggles for the total source term.

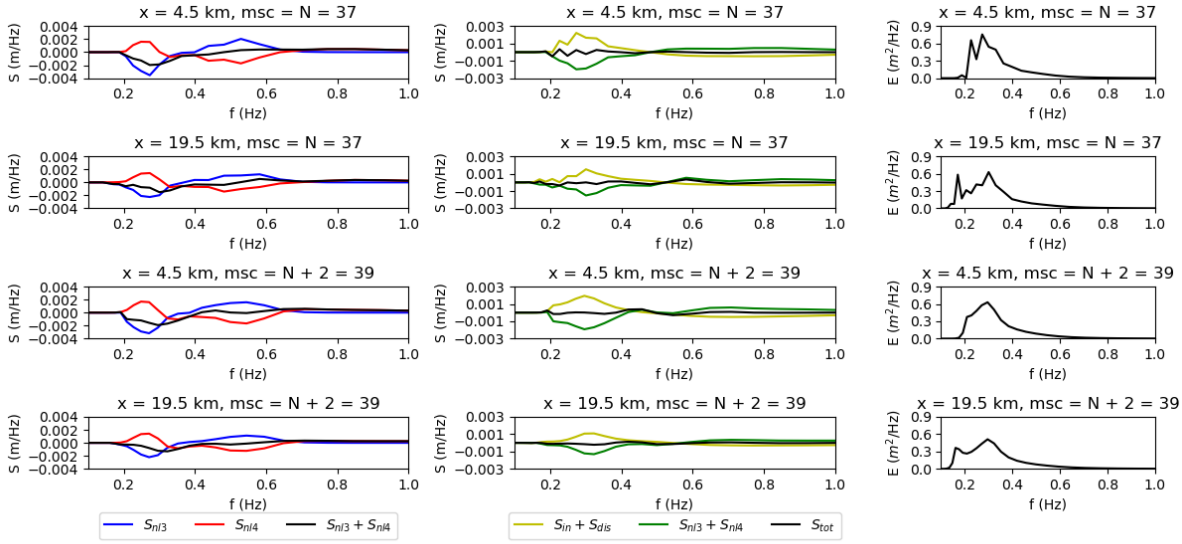

Figure 5.9: Source terms for varying spectral resolutions for $f_{low} = 0.08$ Hz at $U_{10} = 40$ m/s.

Lowering the minimum frequency of the domain also shows improvements of model results, as shown in figure 5.10. The spectrum shows similar features with less wiggles and a lower secondary peak at the low frequency tail. However, earlier results showed how slight alterations in the grid point distribution produced similar results. It is therefore possible that the improvements of using $f_{low} = 0.03$ Hz are not produced by the lower limit itself, but indirectly by the resulting changed distribution of grid points.

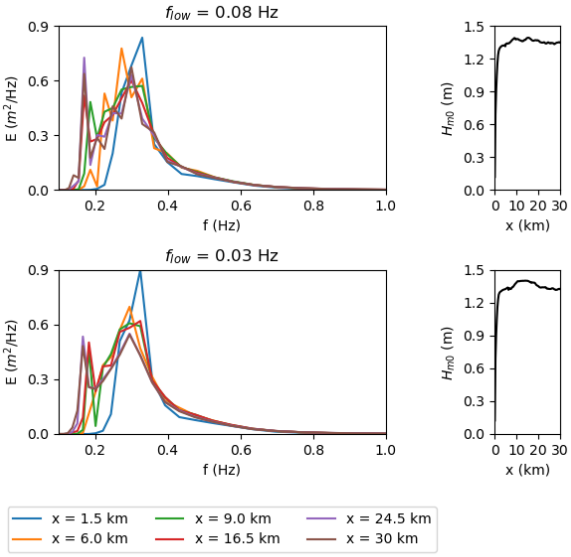

Figure 5.10: Energy density spectra with different lower frequency limits for $U_{10} = 40$ m/s.

5.5. action limiter [limiter]

The wave spectrum is strongly affected by source term interactions. Increasing or decreasing source terms (such as the shallow water source terms) showed to affects the spectrum and the forming of the secondary energy peak. Therefore, the effect of varying the action limiter is also considered using limits of 1 % to 20 %, as shown in figure 5.11 for U_{10} = 40 m/s. For all spectra, wiggles still emerge and it is observed that the significant wave height fails to converge for lower limit values. Varying the action limiter for U_{10} = 20 m/s had no significant effect on the wave spectra and the corresponding source terms.

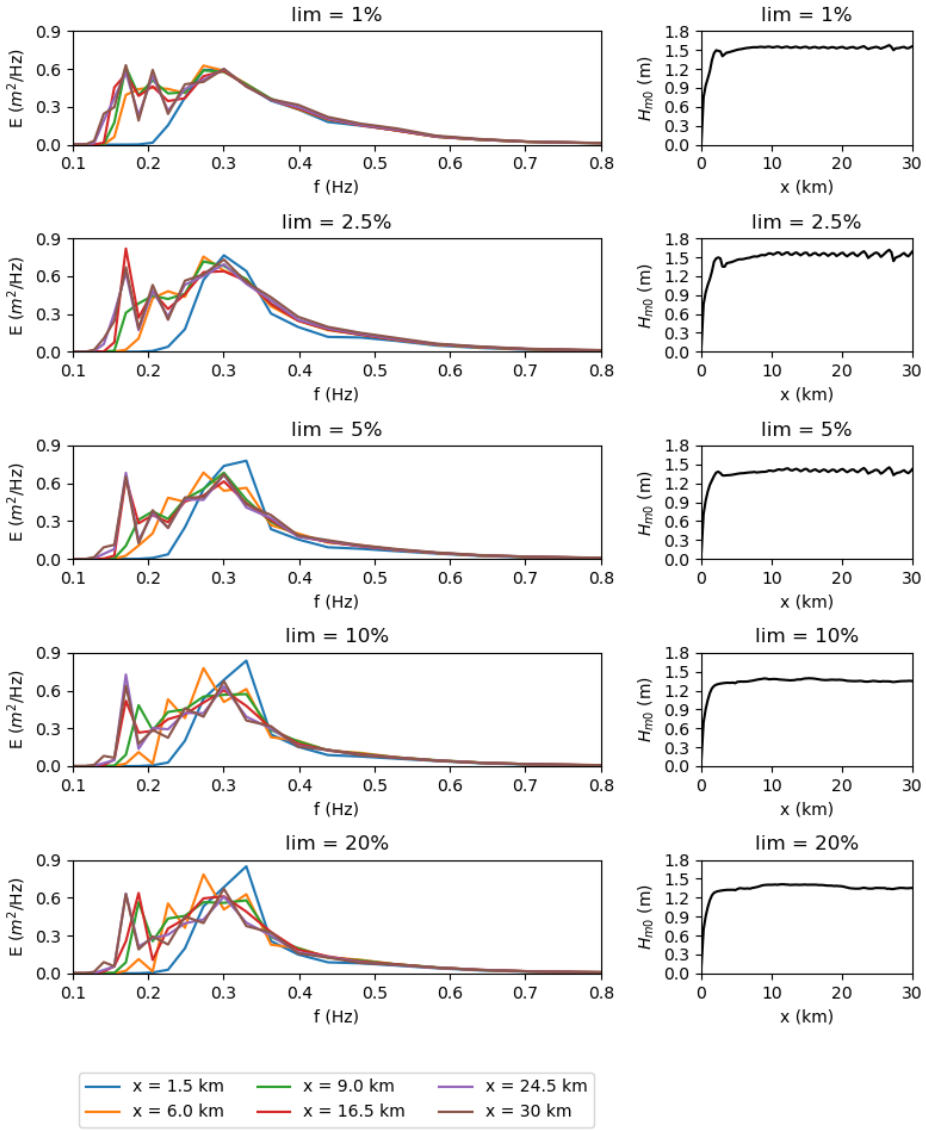

Figure 5.11: Energy density spectra for varying action limits for U_{10} = 40 m/s at several locations.

Inspection of the total energy transfers per source term for high wind speeds along the lake shows periodic behaviour of energy transfers, where source terms alternate between increasing and decreasing (figure 5.12). Especially the depth-induced wave breaking source term varies strongly and it out of phase with the other source terms: the wind input term, the wave-wave interactions and white-capping increase at the same time as the spectrum develops, until wave breaking kicks in. After this, dissipation by wave breaking increases and the other source terms start to decrease. This interactions alternates and is strengthened by lower limiter values. Furthermore, it is observed that increased limiting of the action results in more dominant quadruplet

wave-wave interactions and reduced triad wave-wave interactions.

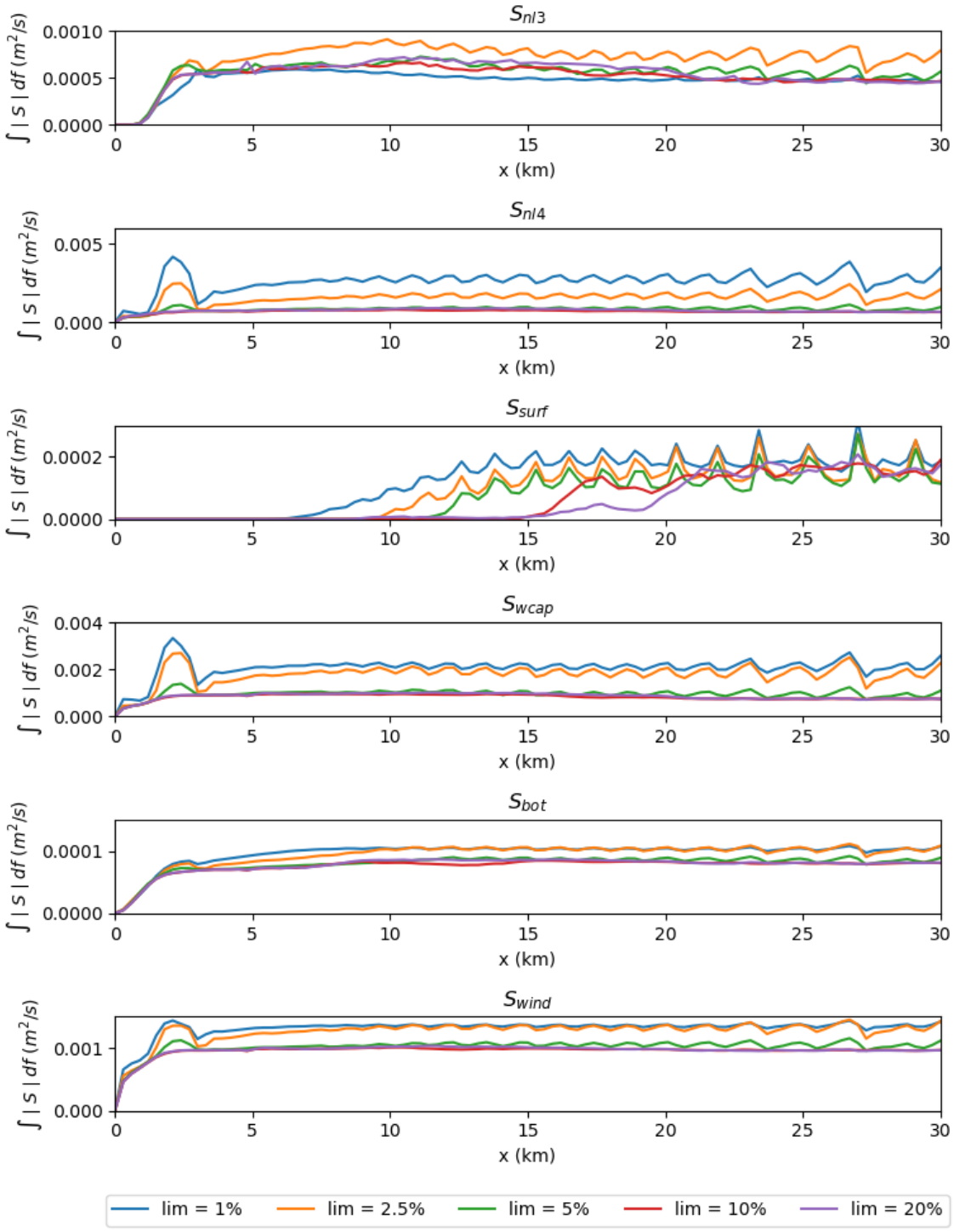

Figure 5.12: Total energy transfers of the source terms for varying action limits for U_{10} = 40 m/s along the lake.

Closer inspection of such an oscillation of the source terms around $x = 26km$ (figure 5.13) shows that the quadruplet source term is dominant and prevents convergence. A strong dip in the total source term emerges simultaneously with an increase in magnitude of the quadruplet source term and shows similar order of

magnitude for a limiter value of 2.5 %. For `[limiter]=10%`, the total source term remains stable and close to zero.

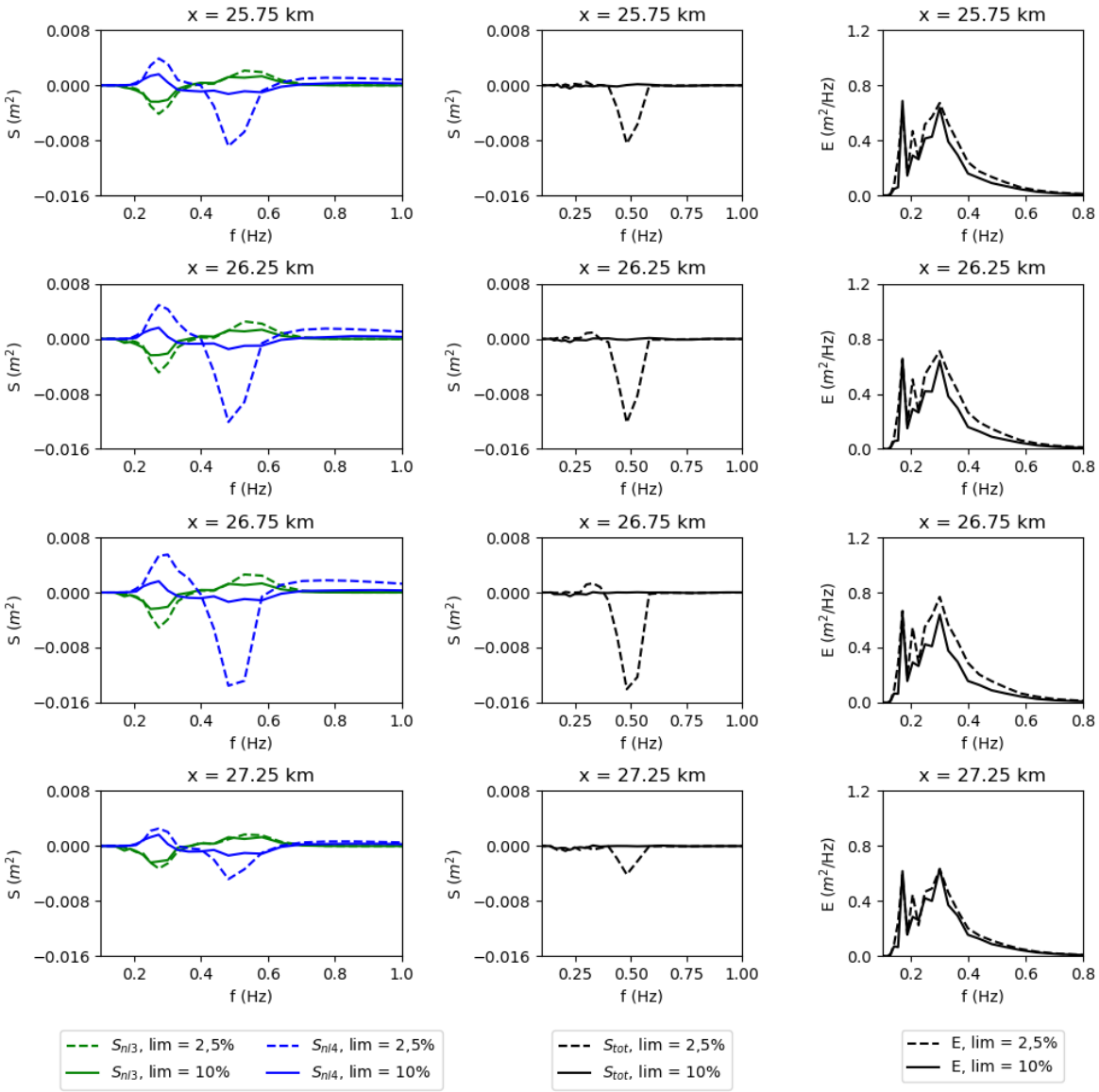

Figure 5.13: Close-up of the source terms of the wave-wave interactions and their effect on the total source term for $U_{10} = 40$ m/s.

6

Discussion

This chapter presents the discussion of the results, taking into account notions presented in academic literature from comparable studies and experiments. First, the link between individual source terms, the wave breaking and triad wave-wave interactions, is explored. Secondly, the interactions all source terms are compared and how they form an equilibrium spectrum, particularly the balance between triad and quadruplet source terms, and the balance between white-capping and depth-induced breaking. Finally, the relation between the frequency resolution and the source term shape is explored.

6.1. Wave breaking and triads

The results demonstrate that varying depth-induced wave breaking parameters in SWAN also affects the triad wave-wave interactions. Both source terms are strongly coupled, but modelling them separately has been proven to be more successful (Salmon et al., 2014). For the BJ78-model (figure 6.1a), a lower breaking parameter γ results in lower redistribution of energy by the triad source term. This is to be expected as a low breaking parameter limits the maximum wave height, which limits nonlinearities through a lower Ursell-number, thus resulting in a lower value of the triad source term. Effectively, setting a low breaking parameter close to the theoretical limit of $\gamma = 0.54$, derived by Nelson (1997), does remove the secondary peak for low frequencies, but also results in an underestimation of the triads and a lower significant wave height. Intuitively, setting a low value for the breaking parameter dampens the wave spectrum and removes wave energy before it can be redistributed, similarly to the conclusion of Van der Westhuysen (2010b) based on the results of lake George observations. As a result, energy is mostly redistributed by the quadruplet source term.

It is possible that heavy wave breaking may weaken or 'destroy' the triad wave-wave interactions (Eldeberky, 1996; Sénéchal et al., 2002; Mahmoudof et al., 2018), but it remains questionable whether this is applicable in the situation of shallow lakes. For example, oceanic waves approaching the surf zone may encounter a sand bar which may rapidly induce wave breaking, similarly to the waves passing a sand bar in the flume in the Eldeberky (1996) experiment. In such cases, dissipation is triggered and the triad source term is lower as a result of the reduces degree of nonlinearity. The situation for shallow water lakes is different as the bottom topography can be nearly horizontal. Waves gradually increase their wave height as a result of wave-wind interactions with consequently increasing nonlinearities, until they become unstable and collapse. As a result, dissipation due to wave breaking is distributed along the whole lake and not concentrated into a single breaking event, and the waves are capable of nonlinear wave-wave interactions until they collapse. It is therefore unlikely to assume that wave breaking should remove the triad wave-wave interactions, as observed in model results with a low constant breaking parameter. Instead, wave breaking may be treated as a general process affecting the whole spectrum through overall energy dissipation (Beji & Battjes, 1993).

Alternatively, a higher constant breaking parameter results in increased triad interactions and results similar to the $\beta - kd$-model for $\gamma = 1.0$ (figure 6.1b). On the other hand, the secondary peak remains emerging for these values and the validity of such a high breaking parameter remains questionable in comparison with results from academic literature, e.g. Battjes & Stive (1985) and Salmon (2016). Particularly, finite depth conditions with a horizontal bottom or barred beaches tend to disagree with the use of a constant breaking

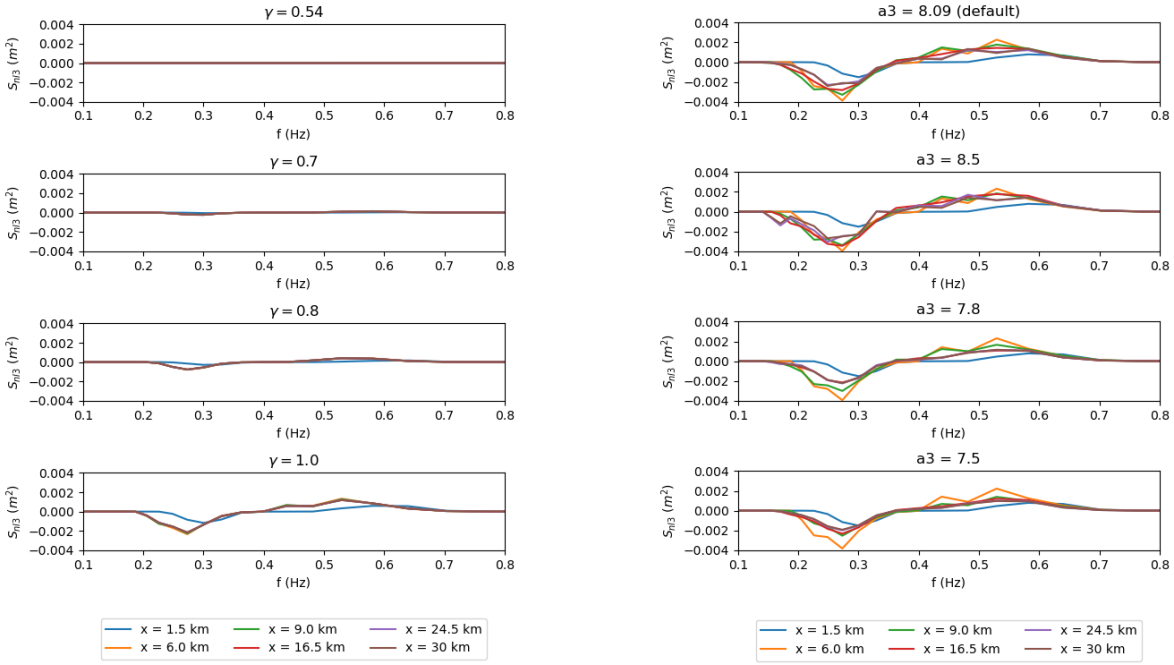

(a) The triad source term using the BJ78-model for varying γ.

(b) The triad source term using the $\beta - kd$-model for varying `[a3]`.

Figure 6.1: Comparison of the triad source term S_{nl3} for U_{10} = 40 m/s at several locations for two wave breaking formulations: the BJ78-model and the $\beta - kd$-model.

parameter (Ruessink et al., 2003; Salmon, 2016), and using the BJ78-model may result in an upper limit for the relative wave height H_{m0}/d (Van Dongeren et al., 2011).

The $\beta - kd$-model is a more promising alternative to adapt wave breaking to the default triad source term. With this model it is still possible to incorporate the theoretical value of $\gamma = 0.54$ for horizontal bottoms while reducing wave breaking of young wind wave, allowing these waves to grow. Comparing the breaking source term S_{br} between the BJ78-model and $\beta - kd$-model for high frequencies indicates less dissipation in the high frequency area for several configurations of the $\beta - kd$-model, thus preventing heavy dampening of the wave spectrum. As a result, both shallow water source terms are active and shape the spectrum: the wave-wave interactions transfer energy from the peak frequency to higher frequencies, and wave breaking dissipates energy from the spectrum.

Comparing these results from the $\beta - kd$-model with surf zone observations from Herbers et al. (2000), we observe again differences in the distribution of wave energy. Herbers et al. (2000) observes that triad interactions are responsible for energy transfer to higher frequencies, which is then followed by dissipation due to wave breaking at these higher frequencies. In contrast, our result of the $\beta - kd$-model show a reduction of dissipation at these higher frequencies, and increased energy transfer by triad and quadruplet wave-wave interactions (see figure 6.2). Correspondingly, the triad source term balances the quadruplet source term which reduces the overall redistribution of energy, and dissipation due to wave breaking occurs along the whole spectrum.

This difference can again be explained by distinctions in bathymetry, as Herbers et al. (2000) observed a sloping beach instead of a shallow near-horizontal lake. For sloping beaches, the gradual decrease of the water depth will result in wave breaking of high-frequency waves until all waves have broken, thus removing the energy transferred to higher frequency waves. Similarly, Mahmoudof et al. (2018) describes the transfer to higher frequencies in the surf zone as a result of wave breaking itself. In the case of our model results for a shallow lake, it is less likely for short waves to quickly break due to depth-induced wave breaking as the water depth remains constant instead of gradually decreasing. Therefore, the high frequency waves are free to develop, to be subjected to quadruplet energy transfer to lower frequencies, or to dissipate as a result of

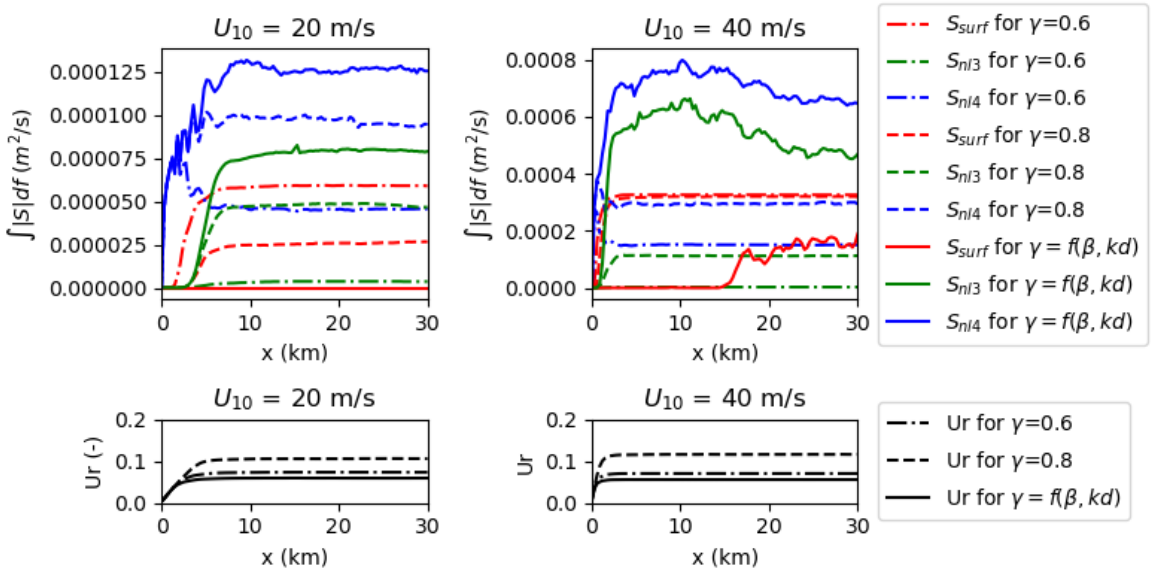

Figure 6.2: The effect of different breaking formulations on the contributions of total energy transfer $\int |S| df$ by depth-induced wave breaking and the nonlinear triad and quadruplet wave-wave interactions.

white-capping. Wave breaking is concentrated around the peak frequency and thus balances the wind input term and affects the longer waves that 'survived' white-capping.

Variations in the `[a3]` parameter for the $\beta - kd$-model show improved results for a lower value of `[a3]`. The low-frequency peak has decreased, the resulting spectrum is more smooth and the triad source term is less spiky. A lower `[a3]` parameter results in a higher breaking parameter for shorter waves, which consequently allows an increased wave height for these young wind waves. As indicated by Salmon (2016), it is important to note that collapsing of waves for these wave $kd > 1$ may still occur as a result of white-capping, and thus dissipation will still occur at higher frequencies.

6.2. Source term balancing

Generally, the wave spectrum is shaped either by the source terms in deep water or by shallow water effects. In deep water, wind waves are generated at the high frequency band and quadruplet wave-wave interactions redistribute wave energy to lower frequencies, until an equilibrium shape is reached (K. Hasselmann, 1974; Holthuijsen, 2007). In the surf zone, wave breaking and triad wave-wave interactions are the dominant processes shaping the wave spectrum (Vink, 2001), but still equilibrium ranges can be identified during wave breaking and the offshore spectral shape is retained (Smith & Vincent, 2002; Smith, 2004). For horizontal bottoms, dissipation is reduced and may even be secondary to the wave-wave interactions in driving the equilibrium shape of the spectrum (Smith, 2004).

Likewise, our model results do show convergence to a stable shape of the spectrum, thus suggesting similarities with these equilibrial features. However, observations of the individual source terms indicate interactions driving the spectral shape which are different than those in oceanic waters or the surf zone. The triad wave-wave interactions, a shallow water source term, are balanced by the deep water quadruplet wave-wave interactions ($S_{red} = S_{nl3} + S_{nl4}$), and the wind input term (S_{in}) balances the dissipative terms of wave breaking, white-capping and bed friction (S_{dis}). This is especially the case for runs with a low proportionality factor for the triad source term (`trfac = 0.05`, see figure 6.3); a higher factor (`trfac=0.8`) produces source terms with more spikes and less balancing.

Furthermore, the source terms depend on the spectral shape and do not distinguish between young wind waves and developed waves; in other words, shallow water processes and deep water processes get 'mixed up' as they are all of similar order of magnitude and do not dominate each other. Intuitively, one could expect that the wave field contains a wide range of waves with low and high relative depths. Wind waves

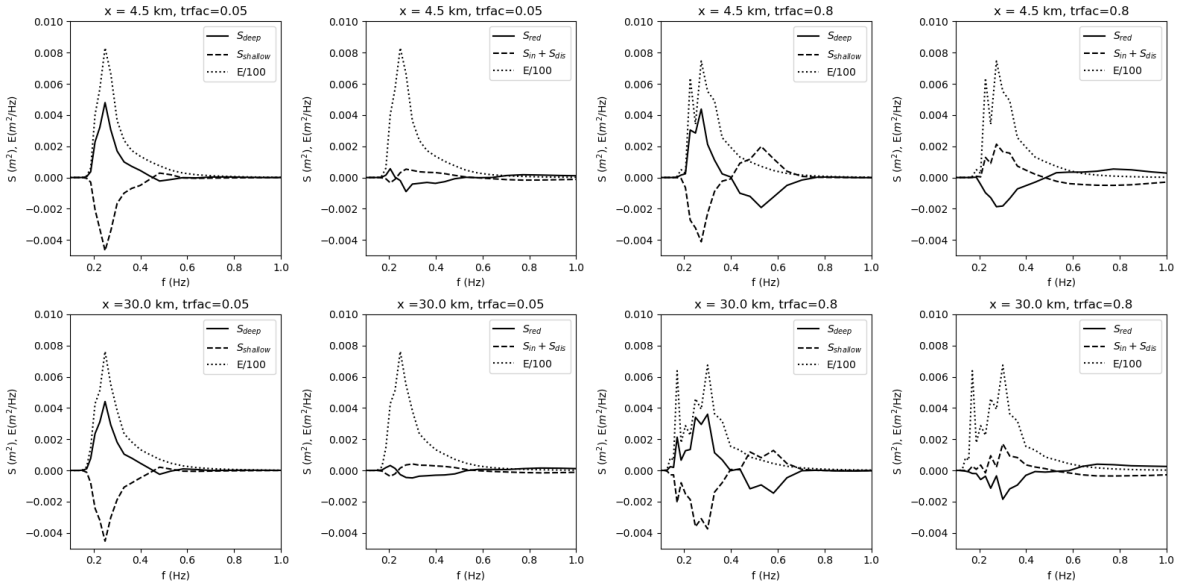

Figure 6.3: Comparison of source term balancing for different proportionality factors for the triad source term using the $\beta - kd$-model for wave breaking at U_{10} = 40 m/s. S_{deep} consists of the deep water source terms (wind input, white-capping, quadruplets) and $S_{shallow}$ the remaining shallow water source terms (depth-induced breaking, friction, triads). S_{in} contains the wind-input term, S_{diss} the dissipative terms (white-capping, friction and breaking) and S_{red} the triad and quadruplet nonlinear wave-wave interactions responsible for redistributing the wave energy. A scaled energy density spectrum $E(f)/100$ at the location is also included.

are generated in the short-wave section of the spectrum, and energy is transferred to lower frequencies by the quadruplets. As waves get higher and longer, they eventually break as a result of the limited relative water depth, while generation of short waves by wind continues, especially for high wind speeds. This makes it difficult to determine whether the source terms represent these separate processes.

Reducing of removing the triad source term results in smooth results with no secondary energy peak, as suggested by Groeneweg & Gautier (2020) and confirmed by our results. However, this measure may not correctly represent the physics taking place in shallow lakes. As the spectrum develops, the peak frequency and thus the mean wave number decreases, which would favour the activation of triad wave-wave interactions as the water gets 'shallower' for the waves.

Alternatively, several authors argue that the quadruplet energy transfer may even be limited for low wave numbers (Zakharov, 1999; Van der Westhuysen, 2007; P. Janssen & Onorato, 2007; Kashima & Mori, 2019) with a proposed limit of $kd = 1.363$. As a solution, Van der Westhuysen (2007) proposes to deactivate quadruplet interactions in strongly nonlinear wave field based on the Ursell number (for example, $Ur > 0.1$). van Vledder & Bottema (2003) show that the standard formulation of the quadruplet DIA term in shallow water may induce larger energy transfers to the low frequency tail of the spectrum, as observed in our results. Therefore, reducing the quadruplet source term may improve model results and reduce the emergence of the secondary low frequency peak in the spectrum. However, Bottema (2001) argues that partial deactivation of quadruplet interaction can lead to poor iteration behaviour in some situations.

It may seem attractive to deactivate quadruplets in shallow water and triads in deep water. Nonetheless, this example demonstrates that waves with high and low kd are present in the wave field, thus showing the importance of both shallow and deep water source terms, and deactivation of all nonlinear terms would oversimplify the model. Additionally, lowering the proportionality factor of the triad source term is possible, but this poses similar disadvantages as deactivating the term as it may underestimate the effect of the triads on the spectrum and calibration and verification may be necessary.

Similarly to nonlinear wave-wave interactions, wave breaking may be present in both shallow and deep water, namely through the white-capping and depth-induced wave breaking source terms. Generally, the application of each source term is distinct and based on specific physical processes: white-capping is wind-driven

while depth-induced wave breaking occurs for limited water depths. Still, both terms describe dissipation of energy as a result of the collapse of the unstable wave crest and the question can be raised whether both source terms may be complementary for waves in very shallow water, especially for high wind speeds where waves grow rapidly and thus white-capping is expected.

Comparing results of both source terms (figure 6.4) shows that white-capping reduces when depth-induced breaking starts to occur. Furthermore, a larger breaking parameter results in more white-capping and less wave breaking, and the combined dissipation ($S_{wcap}+S_{surf}$) increases as total depth-induced breaking reduces. However, these variations are smaller when comparing results obtained using the $\beta - kd$-model for wave breaking, even though the difference between the source terms ($S_{wcap} - S_{surf}$) varies as `[a3]` is altered.

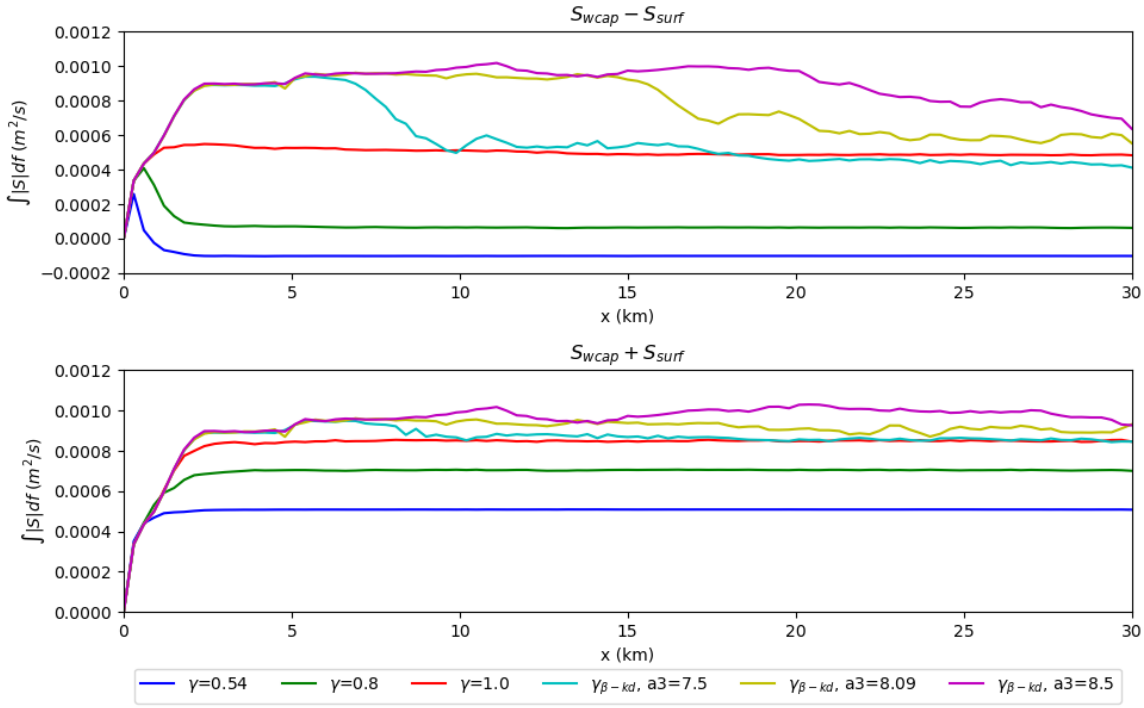

Figure 6.4: Comparison between the dissipation for the white-capping and depth-induced breaking source terms for several wave breaking formulations at $U_{10} = 40$ m/s.

6.3. Effect of numerical variations on source term shape

The SWAN results show how the source terms are affected by the resolution of the frequency domain of the model. Most source terms are of the same order of magnitude but differ in shape, even when some terms are a function of the spectrum $E(f)$. This is especially noticeable in the case of the nonlinear source terms where the magnitude and shape are opposite but similar and as a result, opposing peaks may cancel out when the corresponding frequencies coincide. However, a low frequency resolution may limit the availability of grid points and therefore result in different frequencies for these peaks preventing that they cancel out. Consequently, the sum of these term becomes 'spiky' instead of smooth, as observed in figure 5.9. Increasing the frequency resolution clearly improves these model results.

However, the quadruplet source term has carefully been calibrated for $\Delta f/f = 0.1$, and variations in this source term has shown to have large effects on the development of the wave spectrum. For increased action limiters, the quadruplet source term becomes unstable which affects the total source term and thus the whole spectrum. This underlines the importance of correctly calibrating the source terms of the nonlinear wave-wave interactions and how they interact: when a low action limiter disrupts this balance, the solution fails to converge.

7

Conclusion and recommendations

In this study the effects of varying two shallow water source terms has been investigated with the objective to improve results for modelling strong wind waves in shallow lakes. The primary trigger for this investigation has been the emergence of a secondary energy peak near low frequencies at high wind speeds. Initially, it has been suggested that activation of the triad source term could cause this energy peak, and should therefore be reduced by lowering the proportionality factor (Groeneweg & Gautier, 2020; Groeneweg, 2021). As a result, a one dimensional SWAN model has been derived in order to investigate source term interactions and possible suggestions for modelling improvements.

It has been shown that nonlinear effects affects waves and wave-wave interactions, and that such processes can be described using phase-resolving and phase-averaged models. Extension of linear wave theory to include nonlinear effects enables the formulation of source terms describing these processes in models such as SWAN. This has resulted in different models describing depth-induced wave breaking (BJ78-model and $\beta - kd$-model) and triad wave-wave interactions (LTA, SPB and CCA formulations). The original authors of these models have provided parameter values based on calibration and verification, but in practice deviations emerge from these values as the application of these models is extended to different conditions, such as changes in wind, bathymetry and active source terms.

This investigation has demonstrated that modelling of triad wave-wave interactions and depth-induced breaking in shallow lakes can become problematic for high wind speeds. Deep water and shallow water source terms strongly interact, and distinctions between physical processes become difficult to recognize in model results as a consequence of strong source term interactions. Examples of such interactions are white-capping versus depth-induced wave breaking, and the triad and quadruplet wave-wave interactions.

It is possible to produce smoother model results by increasing of decreasing the effects of certain source terms. For example, increased depth-induced wave breaking removes the secondary energy peak, and reduction of triad wave-wave interactions produces smoother results. However, such measures may not correctly represent the physical processes taking place for wind waves in such shallow lakes, as describing wave breaking in shallow flat-bottom waters remains a challenge and triad wave-wave interactions are not expected to be 'destroyed' by wave breaking in our examples. The $\beta - kd$-model for wave breaking, which makes a distinction between types of waves through kd, showed much better results and seems suitable for modelling horizontal bathymetries, such as shallow water lakes. Allowing young wind waves to develop through the use of the $\beta - kd$-model resulted in improved model and improved source term balancing, especially for lower values of [a3].

Furthermore, model results indicate that the quadruplet source term plays an important role in forming the secondary low-frequency peak, and deactivation of this source term for strongly non-linear wave field has been suggested as a solution to improve model results. Therefore, it may be more attractive to investigate the possibilities of reducing the effect of the quadruplet source term in shallow water, instead of lowering the effect of the triads which are, by definition, a shallow water source term.

An alternative and attractive solution is to improve numerical performance as it does not change the default formulation of source terms in SWAN. It has been shown that the action limiter strongly affects the source terms at high wind speeds, and should not be limited too strongly as it enhances oscillations in the quadruplet source term and, consequently, the whole wave spectrum. Increasing the frequency resolution showed promising results and is supported by examples in academic literature. Still, the default resolution is based on calibration of the quadruplet source term, and should therefore be changed with caution: the quadruplet source term has a strong presence in the model results, so changing this term may worsen model results similarly to the reduced performance observed for low action limiter values. Choosing a resolution of $\Delta f/f = 0.05$ may be too drastic compared to the default value of $\Delta f/f = 0.1$; a possible alternative may be to use $\Delta f/f = 0.07$ similarly to Eldeberky & Battjes (1995).

Still, this investigation encountered several limitations and is clearly oversimplified. A wind field with constant wind speed was used, only one dimension was considered and the bathymetry was assumed fully horizontal. Because of these assumptions, effects such as shoaling and refraction are not considered and comparison with real-life measurements is more difficult. Therefore, further investigation may aim to test the suggested improvements in the context of a more realistic 2D model where the performance can be verified by measurements.

Additionally, difficulties were found for modelling wave breaking for horizontal bottoms, and for the representation of the quadruplet source term in shallow water. It may therefore be interesting to investigate such effects in laboratory settings where experiments can be performed in a long, shallow and flat flume, thus allowing investigation of the interaction between wave breaking (depth-induced and white-capping) and wave-wave interactions (triad and quadruplet) in shallow conditions with no clear wave breaking 'trigger' such as a sand bar. In order to correctly incorporate these nonlinear effects, one may resort to the use of nonlinear Boussinesq models for a phase-resolving approach, or the use of bispectral analysis for a phase-averaged approach.

References

Abreu, M., Larraza, A., & Thornton, E. (1992). Nonlinear transformation of directional wave spectra in shallow water. *Journal of Geophysical Research*, *97*. doi: 10.1029/92jc01826

Battjes, J. (1974). Surf similarity. *Proceedings of the 14thInternational Conference onCoastal Engineering*, 467-479. doi: https://doi.org/10.1061/9780872621138.029

Battjes, J., & Groenendijk, H. (2000). Wave height distributions on shallow foreshores. *Coastal Engineering*, *40*, 161-182. Retrieved from www.elsevier.comrlocatercoastaleng

Battjes, J., & Janssen, J. (1978). Energy loss and set-up due to breaking of random waves. *Coastal Engineering*, 569-587.

Battjes, J., & Stive, M. (1985). Calibration and verification of a dissipation model for random breaking waves. *Journal of Geophysical Research: Oceans*, *v90*, 9159-9167.

Becq, F., Benoit, M., & Forget, P. (1998). Numerical simulations of directionally spread shoaling surface waves. *Coastal Engineering Proceedings*.

Becq-Girard, F., Forget, P., & Benoit, M. (1999). Non-linear propagation of unidirectional wave fields over varying topography. *Coastal Engineering*, *38*, 91-113.

Beji, S., & Battjes, J. (1993). Experimental investigation of wave propagation over a bar. *Coastal Engineering*, *19*, 151-162.

Bosboom, J., & Stive, M. (2022). *Coastal dynamics*. Delft University of Technology. doi: 10.5074/T.2021.001

Bottema, M. (2001). *Vooronderzoek numeriek gedrag swan (ministerie van verkeer en waterstaat)*.

Boussinesq, J. (1872). Théorie des ondes et des remous qui se propagent le long d'un canal rectangulaire horizontal, en communiquant au liquide contenu dans ce canal des vitesses sensiblement pareilles de la surface au fond. *Journal de mathématiques pures et appliquées*, 55-108.

Bouws, E., & Komen, G. J. (1983, 9). On the balance between growth and dissipation in an extreme depth-limited wind-sea in the southern north sea. *Journal of Physical Oceanography*, *13*, 1653-1658. doi: 10.1175/1520-0485(1983)013<1653:OTBBGA>2.0.CO;2

Bénit, M. P. (2009). *Formulation and quantification of the distributed collinear triad approximation* .

Canavilles, R. I., & Nogales, M. C. (1949). Protection des ports. *PIANC congress 1949 SII-C4*, 31-80.

Cavaleri, L., Abdalla, S., Benetazzo, A., Bertotti, L., Bidlot, J., Breivik, ... Van der Westhuysen, A. (2018, 10). Wave modelling in coastal and inner seas. *Progress in Oceanography*, *167*, 164-233. doi: 10.1016/j.pocean.2018.03.010

Dietrich, J. C., Zijlema, M., Allier, P. E., Holthuijsen, L., Booij, N., Meixner, J. D., ... Westerink, J. J. (2013, 10). Limiters for spectral propagation velocities in swan. *Ocean Modelling*, *70*, 85-102. doi: 10.1016/j.ocemod.2012.11.005

Dingemans, M. (1994). *Water wave propagation over uneven bottoms* .

Doering, J. C., & Bowen, A. J. (1986). Shoaling surface gravity waves: A bispectral analysis. *Coastal Engineering*, 150-162.

Doering, J. C., & Bowen, A. J. (1995). Parametrization of orbital velocity asymmetries of shoaling and breaking waves using bispectral analysis. *Coastal Engineering*, *26*, 15-33.

Eldeberky, Y. (1996). *Nonlinear transformation of wave spectra in the nearshore* .

Eldeberky, Y., & Battjes, J. (1995). Parameterization of triad interactions in wave energy models. *Proceedings on Coastal Dynamics*.

Gautier, C. (2020). *Consistentie in swan-meren. deltares memo 11205257-007-dsc-0004* (Tech. Rep.). Deltares.

Groeneweg, J. (2021). *Instellingen voor swan modellen meren en benedenrivieren. deltares memo 11206818-025-geo-0001* (Tech. Rep.). Deltares.

Groeneweg, J., & Gautier, C. (2020). *Generieke methode swan modellering voor boi en andere rws toepassingen. deltares memo 11205758-041-geo-0001* (Tech. Rep.). Deltares.

Hasselmann, K. (1974). On the spectral dissipation of ocean waves due to whitecapping. *Boundary-Layer Meteorology*, *6*, 107-127.

Hasselmann, K., Barnett, T., Bouws, E., H., C., Cartwright, D., Enke, K., ... H., W. (1973). Measurements of wind-wave growth and swell decay during the joint north sea wave project (jonswap). *Ergaenzungsheft zur Deutschen Hydrographischen Zeitschrift, Reihe A*.

Hasselmann, K., Janssen, P., & Komen, G. (1994). *Wave-wave interaction.* Cambridge univeristy press.

Hasselmann, K., Munk, W., & MacDonald, G. (1963, 6). Bispectra of ocean waves. *Symposium on Time Series Analysis*, 125-139.

Hasselmann, S., Hasselmann, K., Allender, J., & Barnett, T. (1985). Computations and parameterizations of the nonlinear energy transfer in a gravity-wave spectrum. part ii: Parameterizations of the nonlinear energy transfer for application in wave model. *Journal of Physical Oceanography*, *15*, 1378-1391.

Herbers, T., & Burton, M. (1997, 9). Nonlinear shoaling of directionally spread waves on a beach. *Journal of Geophysical Research: Oceans*, *102*, 21101-21114. doi: 10.1029/97JC01581

Herbers, T., Russnogle, N., & Elgar, S. (2000). Spectral energy balance of breaking waves within the surf zone.

Hofland, B., Chen, X., Altomare, C., & Oosterlo, P. (2017, 5). Prediction formula for the spectral wave period tm-1,0 on mildly sloping shallow foreshores. *Coastal Engineering*, *123*, 21-28. doi: 10.1016/j.coastaleng .2017.02.005

Holloway, G. (1980). Oceanic internal waves are not weak waves. *Journal of Physical Oceanography*, *10*, 906-914.

Holthuijsen, L. (2007). *Waves in oceanic and coastal waters.* Cambridge university press.

Holthuijsen, L., Booij, N., Holthuijsen, L., & Ris, R. (1996). The "swan" wave model for shallow water. *Coastal Engineering*, 668-676. Retrieved from https://www.researchgate.net/publication/267791357

Holthuijsen, L., Booij, N., & Ris, R. (1999). A third-generation wave model for coastal regions, part i, model description and validation. *Journal of Geophysical Research Atmospheres*, *104*, 7649-7666. Retrieved from https://www.researchgate.net/publication/215722037

Janssen, P., & Onorato, M. (2007, 10). The intermediate water depth limit of the zakharov equation and consequences for wave prediction. *Journal of Physical Oceanography*, *37*, 2389-2400. doi: 10.1175/JPO3128 .1

Janssen, T. T. (2006). *Nonlinear surface waves over topography* .

Kashima, H., & Mori, N. (2019, 11). Aftereffect of high-order nonlinearity on extreme wave occurrence from deep to intermediate water. *Coastal Engineering*, *153*. doi: 10.1016/j.coastaleng.2019.103559

Kim, Y. C., Beall, J. M., Powers, E. J., & Miksad, R. W. (1980). Bispectrum and nonlinear wave coupling. *Physics of Fluids*, *23*, 258-263.

Kim, Y. C., & Powers, E. J. (1979). Digital bispectral analysis and its applications to nonlinear wave interactions. *IEEE Transactions on Plasma Science*, *7*, 120-131. doi: 10.1109/TPS.1979.4317207

Komen, G., Hasselmann, S., & Hasselmann, K. (1984). On the existence of a fully developed wind-sea spectrum. *Journal of physical oceanography*, *14*, 1271-1285.

Longuet-Higgins, M. (1963). The generation of capillary waves by steep gravity waves. *Journal of Fluid Mechanics*, *16*.

Longuet-Higgins, M. (1969). On wave breaking and the equilibrium spectrum of w ind-generated waves. *Proceedings of the Royal Society of London. A. Mathematical and Physical Sciences*, *310*, 151-159. Retrieved from https://royalsocietypublishing.org/

Madsen, P. A., Murray, R., & Sorensen, O. R. (1991). A new form of the boussinesq equations with improved linear dispersion characteristics. , *15*, 371-388.

Madsen, P. A., & Sorensen, O. R. (1993). Bound waves and triad interactions in shallow water. *Ocean Engng*, *20*, 359-388.

Mahmoudof, S. M., Badiei, P., Siadatmousavi, S. M., & Chegini, V. (2018, 3). Spectral wave modeling in very shallow water at southern coast of caspian sea. *Journal of Marine Science and Application*, *17*, 140-151. doi: 10.1007/s11804-018-0011-y

Menéndez, A. N., & Norscini, R. (1982). Spectrum of shallow water waves: an analysis. *Journal of the Hydraulics Division*, *108*, 75-94.

Miche, M. (1944). Mouvements ondulatoires de la mer en prodondeur constante ou décrousante. *Annales de Ponts et Chaussées*.

Miles, J. W. (1957). On the generation of surface waves by shear flows. *Journal of Fluid Mechanics*, *3*, 185-204. doi: 10.1017/S0022112057000567

Nelson, R. (1997). Height limits in top down and environments. *Coastal Engineering*, *32*, 247-254.

Olieman, M. (2011). *Keuze golfperiodemaat uit swan. deltares memo.*

Oosterlo, P. (2021). *Rws informatie instellingen voor de driegolfwisselwerkingen (triads) in swan.*

Phillips, O. M. (1957). On the generation of waves by turbulent wind. *Journal of Fluid Mechanics*, *2*, 417-445. doi: 10.1017/S0022112057000233

Ris, R., Holthuijsen, L., & Booij, N. (1999, 4). A third-generation wave model for coastal regions, part ii, verification. *Journal of Geophysical Research Athmospheres*, *104*, 7667-7681. doi: 10.1029/1998jc900123

Ruessink, B. G., Walstra, D. J., & Southgate, H. N. (2003). Calibration and verification of a parametric wave model on barred beaches. *Coastal Engineering*, *48*, 139-149. doi: 10.1016/S0378-3839(03)00023-1

Salmon, J. (2016). *Surf wave hydrodynamics in the coastal environment* . doi: 10.4233/uuid:b038f8a2-d2db-46fc-8419-3141f21faa1c

Salmon, J., Holthuijsen, L., Smit, P., Vledder, G. V., & Zijlema, M. (2014). Alternative source terms for swan in the coastal region. *Coastal Engineering*, 1-13.

Salmon, J., Smit, P., Janssen, T., & Holthuijsen, L. (2016, 8). A consistent collinear triad approximation for operational wave models. *Ocean Modelling*, *104*, 203-212. doi: 10.1016/j.ocemod.2016.06.009

Smith, J. M. (2004). Shallow-water spectral shapes. *Coastal Engineering*, 206-217.

Smith, J. M., & Vincent, C. L. (2002). Application of spectral equilibrium ranges in the surf zone. *Coastal Engineering*, *28*, 269-279.

Stoker, J. (1957). *Water waves: the mathematical theory with applications.*

Stokes, G. (1880). On the theory of oscillatory waves. *Mathematical and Physical Papers*, 197-237.

Sénéchal, N., Bonneton, P., & Dupuis, H. (2002). Field experiment on secondary wave generation on a barred beach and the consequent evolution of energy dissipation on the beach face. *Coastal Engineering*, *46*, 233-247. Retrieved from www.elsevier.com/locate/coastaleng

The SWAN team. (2021). *Swan user manual.* Retrieved from https://swanmodel.sourceforge.io/

Thornton, E. B., & Guza, R. T. (1983). Transformation of wave height distribution. *Journal of Geophysical Research, 88*, 5925-5938. doi: 10.1029/JC088iC10p05925

Tissier, M., & Reniers, A. (2021). *Lecture slides in cie4325 ocean waves.* Faculty of Civil Engineering, TU Delft.

Tolman, H. (1992). Effects of numerics on the physics in a third-generation wind-wave model. *Journal of Physical Oceanography, 22*, 1095-1111.

Van der Westhuysen, A. (2007). *Advances in the spectral modelling of wind waves in the nearshore* .

Van der Westhuysen, A. (2009). Modelling of depth-induced wave breaking over sloping and horizontal beds. *11th International Workshop on Wave Hindcasting and Forecasting*.

Van der Westhuysen, A. (2010a). Improved modelling of wave-current interaction in swan. *Coastal Engineering*.

Van der Westhuysen, A. (2010b). Modeling of depth-induced wave breaking under finite depth wave growth conditions. *Journal of Geophysical Research: Oceans, 115*. doi: 10.1029/2009JC005433

Van Dongeren, A., Van der Westhuysen, A., Groeneweg, J., Van Vledder, G., Lansen, J., Smale, A., ... Wenneker, I. (2011). Spectral wave modelling in tidal inlet seas: Results from the sbw wadden sea project. *Coastal Engineering*.

van Vledder, G., & Bottema, M. (2003, 3). Improved modelling of nonlinear four-wave interactions in shallow water. *Proceedings on International Conference on Coastal Engineering, 28*, 459-472. doi: 10.1142/9789812791306_0040

Vink, A. (2001). *Transformation of wave spectra across the surf zone* .

Vledder, G. V., Zijlema, M., & Holthuijsen, L. (2012). Revisiting the jonswap bottom friction formulation. *Coastal Engineering*, 1-8.

WAMDI Group. (1988). The wam model - a third generation ocean wave prediction model. *Journal of Physical Oceanography, 18*, 1775-1810.

Wu, J. (1982). Wind-stress coefficients over sea surface from breeze to hurricane. *Journal of Geophysical Research, 87*, 9704. doi: 10.1029/jc087ic12p09704

Zakharov, V. (1999). Statistical theory of gravity and capillary waves on the surface of a finite-depth fluid. *European Journal of Mechanics - B/Fluids, 18*, 327-344. doi: https://doi.org/10.1016/S0997-7546(99)80031-4

Zijlema, M., & Van der Westhuysen, A. (2005, 3). On convergence behaviour and numerical accuracy in stationary swan simulations of nearshore wind wave spectra. *Coastal Engineering, 52*, 237-256. doi: 10.1016/j.coastaleng.2004.12.006

Zijlema, M., Vledder, G. V., & Holthuijsen, L. (2012, 7). Bottom friction and wind drag for wave models. *Coastal Engineering, 65*, 19-26. doi: 10.1016/j.coastaleng.2012.03.002